Compatibility Issues With Irregular Current Injection Islanding Detection Methods in Multi-DG Units Equipped With Grid-Connected Transformers

Menghua Liu, Wei Zhao, Qing Wang, *Senior Member, IEEE*, Zhiming Wang, Caijun Jiang, Jie Shu, Hao Wang, and Yu Bai

***Abstract*—Compatibility issues with irregular current injection islanding detection methods are actually the problem that some irregular currents at the same frequency injected into the same line may cancel each other out and then the islanding detection may be impaired, which have been discussed under direct couple conditions (i.e., conditions without grid-connected transformers) in the literature. This article analyzes the issues under the opposite conditions where distributed generation (DG) units are equipped with grid-connected transformers, and is aimed at finding a solution. The analysis derives the setting formulas of key parameters for both three-phase and single-phase DG units, and shows that considering fault tolerance and practicability, only specific frequencies can be used for irregular currents. The usable frequencies are different under different cases. These conclusions are different from those based on direct couple conditions. By summarizing the conclusions based on conditions with grid-connected transformers achieved in this article and those based on direct couple conditions in the literature, a complete solution to compatibility issues is obtained. The conclusions in this article have been verified by the experiments and simulations at the end of this article.**

***Index Terms*—Current control, distributed power generation, fault diagnosis, fault tolerant control, islanding, inverters.**

I. Introduction

DISTRIBUTED generation (DG), such as solar and wind turbine generation, has been very popular and attracting more and more research for its flexibility and cleanliness for environment. As a fault diagnosis function in DG, islanding detection has become more important along with the growing penetration rate of DG. A lot of islanding detection methods have been proposed till now, which are generally classified into local methods and remote methods. Local methods include active methods and passive methods, and active methods are focused all the time due to their reliability and cost-effective performance.

One type of active methods is to inject harmonic currents, negative sequence currents, pulse currents, or some other irregular currents into the grid, and identify an island according to the resultant voltage response. Such methods are called irregular current injection islanding detection methods in this article, which will be mainly discussed.

A. Review of Islanding Detection Methods

Researchers have developed a large number of irregular current injection methods through employing various irregular currents and observing different kinds of voltage responses (e.g., harmonic voltages and network impedance). In [1], a special implementation for harmonic injection was introduced and demonstrated via an example based on second harmonic. In [2], second harmonic was injected and a set of parameters based on harmonic voltages were formed to determine an island. Harmonic currents were also used while network impedance was detected and used as the island index in [3], and the special part was that dual-harmonic currents were used to cope with the grid impedance unbalanced condition. Network impedance was also adopted in [4] while noncharacteristic frequency (e.g., 75 Hz) currents were injected. Wu *et al.* [5] proposed even harmonic currents injection and used the index called harmonic energy to judge an island. An approach that injected asymmetric subharmonics currents and monitored the harmonic voltages change was proposed in [6], which was designed to minimize the pollution to the grid. Moreover, negative sequence currents were often used as well [7], [8]. In [7] and [8], the variations of correlative negative sequence voltages and voltage unbalance factor were measured to sense an island, respectively. Additionally, pulse currents were utilized in [9], which is different from the sinusoidal current injection, but still the voltage response was detected. Besides,

Manuscript received April 2, 2021; revised July 6, 2021 and August 12, 2021; accepted September 24, 2021. Date of publication October 6, 2021; date of current version November 30, 2021. This work was supported in part by Sino-US Green Community DC Microgrid Technology Cooperation Research and Demonstration (2019YFE0120200) and in part by the Special Fund Project for Marine Economic Development of Guangdong Province (GDNRC[2020]020). Recommended for publication by Associate Editor M. Molinas. *(Corresponding authors: Jie Shu; Yu Bai.)*

Menghua Liu, Jie Shu, Hao Wang, and Yu Bai are with the Guangzhou Institute of Energy Conversion, Chinese Academy of Sciences, Guangzhou 510640, China (e-mail: liumh13@tsinghua.org.cn; shujie@ms.giec.ac.cn; wanghao@ms.giec.ac.cn; baiyu@ms.giec.ac.cn).

Wei Zhao is with the State Key Laboratory of Power System, Department of Electrical Engineering,Tsinghua University, Beijing 100084, China (e-mail: zhaowei@tsinghua.edu.cn).

Qing Wang is with the Department of Engineering, Durham University, DH1 3LE Durham, U.K. (e-mail: qing.wang@durham.ac.uk).

Zhiming Wang and Caijun Jiang are with China Nuclear Power Design Company Ltd., Shenzhen 518172, China (e-mail: wangzhiming@cgnpc.com.cn; jiangcaijun@cgnpc.com.cn).

Color versions of one or more figures in this article are available at https://doi.org/10.1109/TPEL.2021.3117879.

Digital Object Identifier 10.1109/TPEL.2021.3117879

irregular voltage injection was also mentioned, although relevant research was not too much [10].

Another classic active method is the frequency shift method, which is very different from the irregular current injection method in principle. This method is aimed at shifting frequency up to the trigger limits through some disturbances. There are various disturbances to implement this method. Some methods disturbed the phases of output currents of inverters, including the well-known Sandia frequency shift method and slip-mode frequency shift method [11]. Some methods disturbed reactive currents/power [12]–[14]. In [15], the disturbance to the rate of change of reactive current was proposed, which basically eliminated the current static error resulting from the frequency shift methods, and then a practical parameter selection scheme was developed.

It is worth mentioning that due to the popularity of numerous digital signal processing tools and artificial intelligence algorithms, many of them are incorporated into passive islanding detection methods. In [16], some features were extracted from terminal voltages and currents by means of discreet Fourier transform and symmetrical components method, and then these features were classified by a long short-term memory network to identify an island. Likewise, in [17], a modified intrinsic mode function was used to extract some features, and then these features were classified by ensemble *k*-nearest neighbor classifier. In [18], quadratic time–frequency decomposition was used for a complex representation of three-phase (TP) signal, and the principles of informative sparse representation-based classification was utilized for judgment. However, it is definite that some regular passive methods have still been developing [19]–[23]. They identified an island by means of the variations of some features presented during the inverters operation.

Additionally, islanding detection in the dc microgrid is also receiving much attention. A passive method and an active method were proposed in [24] and [25], respectively. Choudhury and Jena [24] used the cumulative sum of superimposed impedance for islanding detection. In [25], a small ac voltage was superimposed on the output dc voltage and the frequency possessed voltage positive feedback, whereby the grid voltage would oscillate when an island event occurred.

B. Introduction of Irregular Current Injection Methods

For ease of presentation, this article takes harmonics as the representative of irregular currents. As shown in Fig. 1, under grid-connected conditions, the equivalent network impedance $Z_{\rm eq}$ seen from a DG unit is

$$Z_{\rm eq(grid)} = Z_{\rm load} // Z_{\rm grid}$$

where $Z_{\rm load}$ and $Z_{\rm grid}$ denote the load impedance and grid impedance, respectively. Under island conditions in which the grid and $Z_{\rm grid}$ are cut out, $Z_{\rm eq}$ seen from a DG unit is

$$Z_{\rm eq(island)} = Z_{\rm load}.$$

Since $Z_{\rm grid}$ is generally much smaller than $Z_{\rm load}$, $Z_{\rm eq(grid)}$ is much smaller than $Z_{\rm eq(island)}$. In other words, there is a surge of $Z_{\rm eq}$ when an island event occurs. Irregular current injection methods utilize this surge to perceive the island. However, $Z_{\rm eq}$ cannot be directly measured. Thus, an irregular current is generally injected into the grid, and then $Z_{\rm eq}$ can be calculated by measuring the resultant irregular voltage. In the meanwhile, the irregular voltage will also surge due to the surge of $Z_{\rm eq}$ when an island event occurs. Therefore, the irregular voltage is crucial to irregular current injection methods.

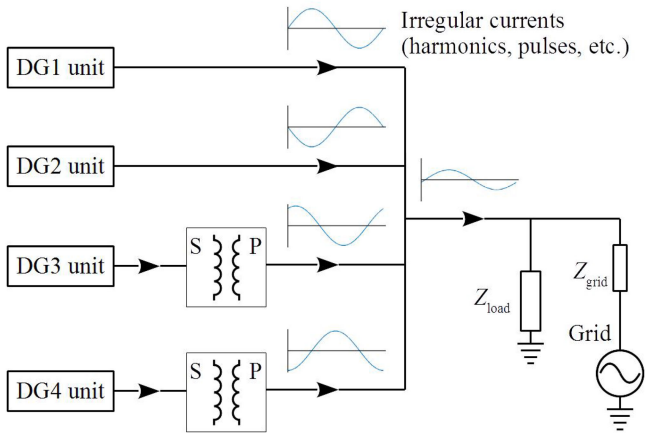

Fig. 1. Injection of multi-irregular currents and their converging.

C. Introduction of Compatibility Issues With Irregular Current Injection Methods

According to the introduction in the previous section, irregular current injection methods are almost impeccable in single-DG operation. However, multi-DG operation is much more common in reality, which is a challenge for irregular current injection methods. As shown in Fig. 1, since the DG units generally do not communicate with each other, the phases of their injected irregular currents are independent and uncoordinated, just like the four waveforms on the left, which may cause the irregular currents to cancel each other out and then cause the converged irregular current to decrease in amplitude, like the waveform on the right. If the converged irregular current is too small to cause a surge of the irregular voltage when an island event occurs, the island cannot be detected. This is just the compatibility issue with irregular current injection methods [26]. The solution to the compatibility issue is to make the converged irregular current increase in any case, which is essential to irregular current injection methods.

Additionally, as irregular currents with different frequencies do not cancel each other out and do not need to be discussed, in this article, the irregular currents injected into the same line have the same frequency.

D. Compatibility Requirement

In order for irregular current injection methods to be compatible with each other, the phase difference between any two irregular currents injected into the same line should be in $[-\pi/2, \pi/2]$, which has been concluded in [26], and the optimal condition is that the phase difference is zero and the irregular currents are in phase.

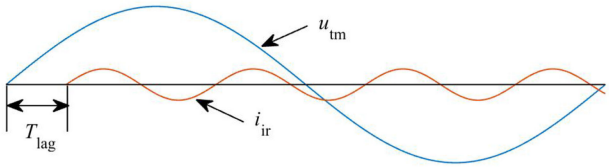

Fig. 2. Injection pattern of an irregular current.

A solution to compatibility issues must satisfy the above-mentioned compatibility requirement. Moreover, the solution is also subject to application conditions considering practicability. First, there is generally no communication between DG units; second, DG units may belong to different owners/users in a zone and the inverters thereof may come from different manufacturers, whereby it is impracticable to uniformly manage all the DG units through an upper level system, particularly for those plug-and-play DG units; finally, to control costs, hardware should not be added, or the solution does not make much sense and will not be popular. This shows that the compatibility issue is difficult to cope with.

E. Solution to Compatibility Issues Under Direct Couple Conditions

In [26], compatibility issues based on direct couple conditions, i.e., conditions without grid-connected transformers (like the DG1 and DG2 units in Fig. 1), were discussed in detail and a solution was proposed finally. The solution mainly included the following two points.

1) Injection Pattern Specially Designed: To coordinate the injection of irregular currents, in [26], the terminal voltages of DG units, i.e., the grid voltage, are suggested as the reference voltages to conduct the injection. In [26], an irregular current is injected in this pattern: the first zero phase of the irregular current i_{ir} lags a zero phase of the terminal voltage u_{tm} (i.e., reference voltage) by T_{lag} (time), which is less than the periods of both i_{ir} and u_{tm}, as shown in Fig. 2. The analysis in this article is still based on this injection pattern.

2) Usable Frequencies for Irregular Currents: In [26], according to the aforementioned injection pattern and considering fault tolerance, the usable frequencies for irregular currents are limited, as shown in the following, where f_{iir} and f_{u} denote the irregular current frequency and terminal voltage frequency, respectively, and q is a positive integer

$$\begin{cases} f_{\mathrm{iir}} = (3q+1)f_{\mathrm{u}}, \\ \text{for three – phase positive sequence currents} \\ f_{\mathrm{iir}} = (3q-1)f_{\mathrm{u}}, \\ \text{for three – phase negative sequence currents} \end{cases} \tag{1a}$$

$$f_{\mathrm{iir}} = (3q \pm 1)f_{\mathrm{u}}, \text{ for single – phase currents.} \tag{1b}$$

Moreover, according to the relevant formulas derived in [26], once the above frequencies are adopted, the TP irregular currents in a TP terminal will spontaneously have the same T_{lag}. This conclusion is actually universal and will be used by the following sections.

F. Topic on Compatibility Issues Under Conditions With Grid-Connected Transformers

In reality, some DG units may be equipped with grid-connected transformers, just like DG3 and DG4 units in Fig. 1. These DG units generally only control their terminal irregular currents, i.e., the secondary irregular currents of the transformers, whose reference voltages are the secondary voltages. However, for compatibility issues, primary irregular currents are the ones that need to be controlled. The phases of primary irregular currents may be different from those of secondary irregular currents, whereas their reference voltages change to the primary voltages. Hence, it is necessary to discuss compatibility issues under conditions with grid-connected transformers.

Throughout the relevant literature, only Liu *et al.* [26] systematically discussed compatibility issues although some other literature has raised similar issues earlier [27]–[29]. Nonetheless, Liu *et al.* [26] only analyzed the issues under direct couple conditions. The work in [26] and the other literature have not mentioned the compatibility issues under conditions with grid-connected transformers. In view of this, this article will focus on this topic and discuss how DG units inject irregular currents to satisfy the compatibility requirement under conditions with grid-connected transformers. The ultimate goal of this study is to obtain a complete solution to compatibility issues, which will extremely improve the effectiveness and reliability of irregular current injection methods in multi-DG operation.

G. Application of the Solution to Compatibility Issues

Once the aforementioned compatibility requirement is met by implementing the solution, the irregular currents will present synchronicity in phase, which may result in some problems such as voltage flicker [27]. As regards voltage flicker, standard EN 61000-3-3 has specified the maximum limits for both short-term and long-term flicker severity [30]. However, the mechanisms of active islanding detection methods are destined to degrade power quality. To balance the performance of irregular current injection methods and power quality, the magnitudes of irregular currents should be severely restricted.

Since the grid is a voltage source, in generation, the inverters built into DG units essentially control the regular currents (i.e., positive sequence fundamental frequency currents) regardless of the control mode (e.g., *P*–*Q* control and droop control). In other words, any type of inverters (i.e., voltage/current source, with/without unfolder, single-/multistage, with/without dc-link, etc.) must be able to accurately control the amplitude, frequency, and phase of a regular current [31]–[34]. Thus, in theory, they can also accurately control irregular currents. It will be seen that as the solution proposed in this article is to choose appropriate frequencies and phases for irregular currents, it is independent of the inverter type. In other words, once the frequencies and phases are determined, any type of inverters can output the expected irregular currents.

This article only studies irregular current injection, which will not be affected by the grid, and does not involve the other aspects of irregular current injection methods. Therefore, the proposed solution is applicable for both stiff and weak grids. However, the

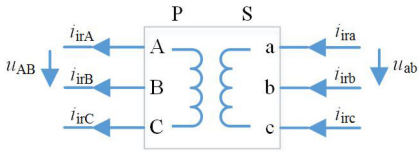

Fig. 3. Irregular currents in a TP transformer.

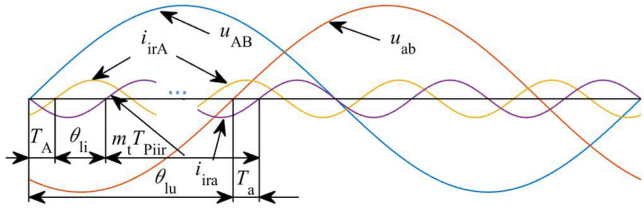

Fig. 4. Injection of the primary and secondary line currents.

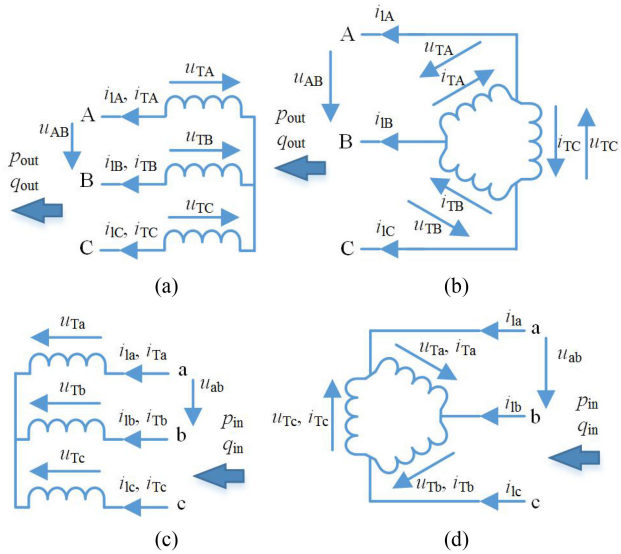

Fig. 5. Voltages and currents based on different windings. (a) Primary winding Y-connection. (b) Primary winding D-connection. (c) Secondary winding y-connection. (d) Secondary winding d-connection.

increasing penetration level of DG units will result in a weak grid whose $Z_{\rm grid}$ is relatively large. Thereupon, according to Section I-B, $Z_{\rm eq(grid)}$ is no longer always much smaller than $Z_{\rm eq(island)}$, which will probably degrade the effect of irregular current injection methods.

The rest of this article is organized as follows. Section II analyzes the relationship between $T_{\rm lag}$ of primary and secondary irregular currents in an ideal transformer, which is a key basis for subsequent analysis. Considering compatibility issues, Sections III and IV study the constraints on irregular currents under normal conditions and fault conditions, respectively. Section V discusses the precautions for actual transformers regarding the compatibility issue and proposes a final complete solution. Section VI verifies the above-mentioned solution via experiments and simulations. Finally, Section VII concludes this article.

II. Relationship Between $T_{\rm LAG}$ of Primary and Secondary Irregular Currents in an Ideal Transformer

A. Relationship Between T_{lag} of Primary and Secondary Irregular Currents in an Ideal TP Transformer

As shown in Fig. 3, the irregular currents injected into the secondary winding, i.e., $i_{\rm ira}$, $i_{\rm irb}$, and $i_{\rm irc}$, will induce $i_{\rm irA}$, $i_{\rm irB}$, and $i_{\rm irC}$ in the primary winding. The reference voltages of $i_{\rm ira}$, $i_{\rm irb}$, and $i_{\rm irc}$ are $u_{\rm ab}$, $u_{\rm bc}$, and $u_{\rm ca}$, respectively, and $T_{\rm lag}$ are expressed as $T_{\rm a}$, $T_{\rm b}$, and $T_{\rm c}$, respectively [26]. Likewise, $T_{\rm lag}$ of $i_{\rm irA}$, $i_{\rm irB}$, and $i_{\rm irC}$ to the reference voltages $u_{\rm AB}$, $u_{\rm BC}$, and $u_{\rm CA}$ are expressed as $T_{\rm A}$, $T_{\rm B}$, and $T_{\rm C}$, respectively.

1) General Formula Between T_a *and* T_A*:* As shown in Fig. 1, if a DG unit and its grid-connected transformer are seen as a whole, the irregular currents injected into the grid, i.e., the primary irregular currents, should have the same characteristics as those directly injected (i.e., without transformers). Accordingly, from the analyses based on direct couple conditions in [26], we can obtain the relationship between $T_{\rm A}$, $T_{\rm B}$, and $T_{\rm C}$ and conclude that $T_{\rm B}$ and $T_{\rm C}$ are determined by $T_{\rm A}$. Therefore, the following discussion will focus on $T_{\rm lag}$ of phase a/A irregular currents, such as $T_{\rm a}$ and $T_{\rm A}$.

In accordance with Fig. 3, the injection of $i_{\rm ira}$ and $i_{\rm irA}$ is shown in Fig. 4, where it is supposed that $u_{\rm AB}$ leads $u_{\rm ab}$ by $\theta_{\rm lu}$ and $i_{\rm irA}$ leads $i_{\rm ira}$ by $\theta_{\rm li}$.

The following equation can be obtained from Fig. 4:

$$T_{\rm Pu}\theta_{\rm lu}/(2\pi) + T_{\rm a} = T_{\rm Piir}\theta_{\rm li}/(2\pi) + T_{\rm A} + m_{\rm t}T_{\rm Piir} \quad (2)$$

where $T_{\rm Pu}$ and $T_{\rm Piir}$ are the periods of the reference voltage and irregular current, respectively, i.e., $1/f_{\rm u}$ and $1/f_{\rm iir}$, and $m_{\rm t}$ is a positive integer and each positive integer may be the value of $m_{\rm t}$.

For a transformer, $\theta_{\rm lu}$ is determined by its winding connection and can be represented by the clock position $N_{\rm clk}$ (e.g., 11 in winding connection symbol Y,d11) of the winding connection symbol, as shown in the following:

$$\theta_{\rm lu} = N_{\rm clk}\pi/6.$$

By substituting the above equation into (2), the following equation can be derived:

$$T_{\rm A} = T_{\rm a} - [(\theta_{\rm li}/\theta_{\rm lu} - f_{\rm iir}/f_{\rm u})N_{\rm clk} + 12m_{\rm t}]/(12f_{\rm iir}). \quad (3)$$

2) Relationship Between θ_{lu} *and* θ_{li}*:* As shown in Fig. 5, $p_{\rm out}$ and $q_{\rm out}$ are the output instantaneous active power and reactive power, $p_{\rm in}$ and $q_{\rm in}$ are the input instantaneous active power and reactive power, $u_{\rm TA}/u_{\rm TB}/u_{\rm TC}$, $i_{\rm TA}/i_{\rm TB}/i_{\rm TC}$ and $i_{\rm lA}/i_{\rm lB}/i_{\rm lC}$ are the primary phase voltages, currents, and line currents, and $u_{\rm Ta}/u_{\rm Tb}/u_{\rm Tc}$, $i_{\rm Ta}/i_{\rm Tb}/i_{\rm Tc}$, and $i_{\rm la}/i_{\rm lb}/i_{\rm lc}$ are the secondary phase voltages, currents, and line currents.

a) Positive sequence currents and voltages at the same frequency: As shown in Fig. 5, since the input active and reactive power of an ideal transformer are equal to the output active and reactive power, respectively, its secondary power factor angle is also equal to the primary power factor angle. Thus, the following

equation is true:

$$\varphi_{\mathrm{uTA}} - \varphi_{\mathrm{iTA}} = \varphi_{\mathrm{uTa}} - \varphi_{\mathrm{iTa}} \tag{4}$$

where φ_{uTA}, φ_{iTA}, φ_{uTa}, and φ_{iTa} are the initial phases of u_{TA}, i_{TA}, u_{Ta}, and i_{Ta}, respectively. As for φ_{uTA} and φ_{iTA} in Fig. 5(a), the following is true:

$$\begin{cases} \varphi_{\mathrm{uTA}} = \varphi_{\mathrm{uAB}} - \pi/6 \\ \varphi_{\mathrm{iTA}} = \varphi_{\mathrm{ilA}} \end{cases}$$

where φ_{uAB} and φ_{ilA} are the initial phases of u_{AB} and i_{lA}, respectively. Then, the following relationship holds:

$$\varphi_{\mathrm{uTA}} - \varphi_{\mathrm{iTA}} = \varphi_{\mathrm{uAB}} - \varphi_{\mathrm{ilA}} - \pi/6. \tag{5}$$

The same relationship as (5) can be derived from Fig. 5(b), and the following relationship can be derived from both Fig. 5(c) and (d):

$$\varphi_{\mathrm{uTa}} - \varphi_{\mathrm{iTa}} = \varphi_{\mathrm{uab}} - \varphi_{\mathrm{ila}} - \pi/6$$

where φ_{uab} and φ_{ila} are the initial phases of u_{ab} and i_{la}, respectively. By substituting (5) and the above equation into (4), the following equation can be derived:

$$\varphi_{\mathrm{uAB}} - \varphi_{\mathrm{uab}} = \varphi_{\mathrm{ilA}} - \varphi_{\mathrm{ila}}. \tag{6}$$

Since $\varphi_{\mathrm{uAB}} - \varphi_{\mathrm{uab}}$ is determined by the winding connection of a transformer and is unrelated to frequency, φ_{ilA}-φ_{ila} is determined by (6) and is also unrelated to frequency. Hence, for a transformer, although (6) is derived from the premise that the voltages and currents have the same frequency, it is still true even if $\varphi_{\mathrm{uAB}} - \varphi_{\mathrm{uab}}$ and $\varphi_{\mathrm{ilA}} - \varphi_{\mathrm{ila}}$ are based on the voltages and currents at different frequencies. Accordingly, considering the definitions of θ_{lu} and θ_{li}, the following equations are given:

$$\begin{cases} \theta_{\mathrm{lu}} = \varphi_{\mathrm{uAB}} - \varphi_{\mathrm{uab}} \\ \theta_{\mathrm{li}} = \varphi_{\mathrm{ilA}} - \varphi_{\mathrm{ila}}. \end{cases}$$

By combining (6) and the above equations, the following equation can be derived:

$$\theta_{\mathrm{li}}/\theta_{\mathrm{lu}} = 1. \tag{7}$$

b) Negative sequence currents and positive sequence voltages at the same frequency: As shown in Fig. 5, according to the instantaneous power theory, the following equation is true [35]:

$$\begin{cases} p_{\mathrm{out}} = 3U_{\mathrm{TA}} I_{\mathrm{TA}} \cos(2\omega t + \varphi_{\mathrm{uTA}} + \varphi_{\mathrm{iTA}} - \pi) \\ q_{\mathrm{out}} = 3U_{\mathrm{TA}} I_{\mathrm{TA}} \sin(2\omega t + \varphi_{\mathrm{uTA}} + \varphi_{\mathrm{iTA}} - \pi) \\ p_{\mathrm{in}} = 3U_{\mathrm{Ta}} I_{\mathrm{Ta}} \cos(2\omega t + \varphi_{\mathrm{uTa}} + \varphi_{\mathrm{iTa}} - \pi) \\ q_{\mathrm{in}} = 3U_{\mathrm{Ta}} I_{\mathrm{Ta}} \sin(2\omega t + \varphi_{\mathrm{uTa}} + \varphi_{\mathrm{iTa}} - \pi) \end{cases} \tag{8}$$

where U_{TA}, I_{TA}, U_{Ta}, and I_{Ta} are the root mean square of u_{TA}, i_{TA}, u_{Ta}, and i_{Ta}, respectively, and ω is the angular frequency. For an ideal transformer, the following equation is true:

$$U_{\mathrm{TA}}/U_{\mathrm{Ta}} = I_{\mathrm{Ta}}/I_{\mathrm{TA}}.$$

As $p_{\mathrm{out}} = p_{\mathrm{in}}$ and $q_{\mathrm{out}} = q_{\mathrm{in}}$, the following equation can be derived from (8) and the above relationship:

$$\varphi_{\mathrm{uTA}} + \varphi_{\mathrm{iTA}} = \varphi_{\mathrm{uTa}} + \varphi_{\mathrm{iTa}}.$$

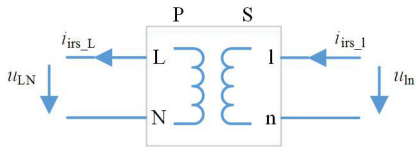

Fig. 6. Irregular currents in an SP transformer.

The above equation is similar to (4). Thus, by following the derivation after (4), the following equation can be derived:

$$\theta_{\mathrm{li}}/\theta_{\mathrm{lu}} = -1. \tag{9}$$

In summary, the relationship between T_{a} and T_{A} can be achieved from (3), (7), and (9), as shown in the following equation:

$$\begin{cases} T_{\mathrm{A}} = T_{\mathrm{a}} - [(1 - f_{\mathrm{iir}}/f_{\mathrm{u}})N_{\mathrm{clk}} + 12m_{\mathrm{t}}]/(12f_{\mathrm{iir}}) \\ \text{for positive sequence irregular currents} \\ T_{\mathrm{A}} = T_{\mathrm{a}} - [(-1 - f_{\mathrm{iir}}/f_{\mathrm{u}})N_{\mathrm{clk}} + 12m_{\mathrm{t}}]/(12f_{\mathrm{iir}}) \\ \text{for negative sequence irregular currents.} \end{cases} \tag{10}$$

B. Relationship Between T_{lag} *of Primary and Secondary Irregular Currents in an Ideal Single-Phase (SP) Transformer*

As shown in Fig. 6, by following the definitions for TP transformers, T_{lag} of $i_{\mathrm{irs\_l}}$ and $i_{\mathrm{irs\_L}}$ to the reference voltages u_{ln} and u_{LN} are expressed as T_{l} and T_{L}, respectively.

From the above analysis for TP transformers, it can be seen that (3) is also applicable for SP transformers when T_{l} and T_{L} are substituted for T_{a} and T_{A}, respectively. As regards the relationship between θ_{lu} and θ_{li}, by following the derivation in Section II-A2-a), from the power factor angle point of view, (7) is still true. Accordingly, the relationship between T_{l} and T_{L} can be achieved, as shown in the following equation:

$$T_{\mathrm{L}} = T_{\mathrm{l}} - [(1 - f_{\mathrm{iir}}/f_{\mathrm{u}})N_{\mathrm{clk}} + 12m_{\mathrm{t}}]/(12f_{\mathrm{iir}}). \tag{11}$$

III. Constraints on Irregular Currents Under Normal Conditions Considering Compatibility Issues

As shown in Fig. 7, since the TP transformer is equipped for DG1 and DG2 units, these two units can acquire the transformer parameters, such as the winding connection symbol (including N_{clk}). Due to superposition theorem, DG1 and DG2 units can be discussed separately regarding irregular currents injection. Therefore, only DG1 unit is discussed, whereas DG2 unit is ignored here. According to the aforementioned compatibility requirement, the aim is only to make the phase difference between $i_{\mathrm{irA\_T1}}/i_{\mathrm{irB\_T1}}/i_{\mathrm{irC\_T1}}$ and $i_{\mathrm{ira3}}/i_{\mathrm{irb3}}/i_{\mathrm{irc3}}$ be in $[-\pi/2, \pi/2]$. Accordingly, for DG1 unit, T_{lag} of its output irregular current $i_{\mathrm{ira1}}/i_{\mathrm{irb1}}/i_{\mathrm{irc1}}$ does not need to be $T_{\mathrm{a}}/T_{\mathrm{b}}/T_{\mathrm{c}}$ like $i_{\mathrm{ira3}}/i_{\mathrm{irb3}}/i_{\mathrm{irc3}}$. Consequently, once T_{lag} of $i_{\mathrm{ira1}}/i_{\mathrm{irb1}}/i_{\mathrm{irc1}}$ is not limited, T_{lag} of $i_{\mathrm{irA\_T1}}/i_{\mathrm{irB\_T1}}/i_{\mathrm{irC\_T1}}$, i.e., $T_{\mathrm{A}}/T_{\mathrm{B}}/T_{\mathrm{C}}$, can be controlled to any value in terms of (10). That being the case, $T_{\mathrm{A}}/T_{\mathrm{B}}/T_{\mathrm{C}}$ can be controlled to $T_{\mathrm{a}}/T_{\mathrm{b}}/T_{\mathrm{c}}$ at all, as the following equation, to make $i_{\mathrm{irA\_T1}}/i_{\mathrm{irB\_T1}}/i_{\mathrm{irC\_T1}}$ be in phase with $i_{\mathrm{ira3}}/i_{\mathrm{irb3}}/i_{\mathrm{irc3}}$, whereby

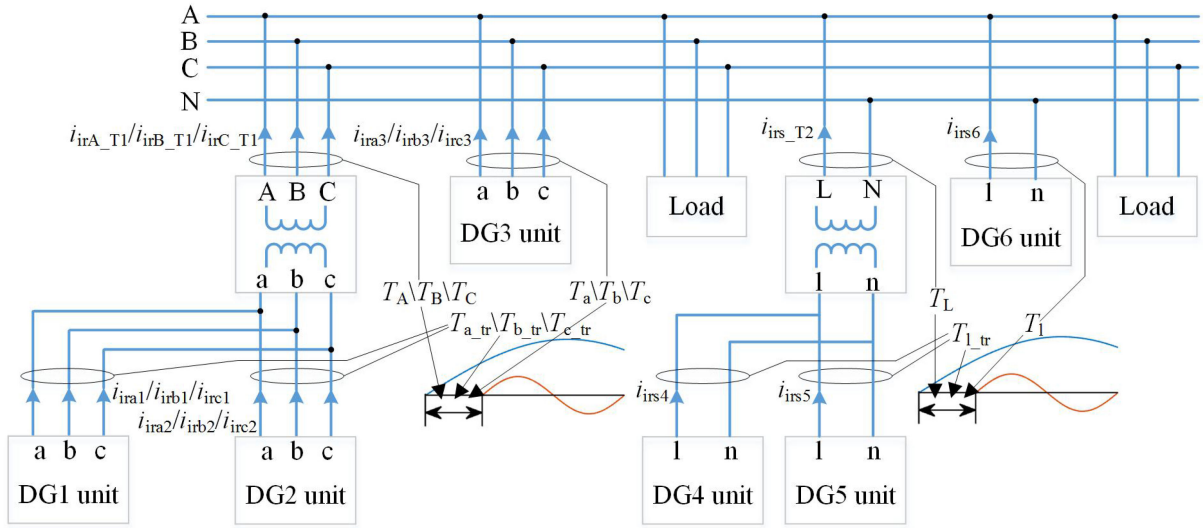

Fig. 7. Setting of T_{lag} under the conditions with transformers.

the optimal condition is achieved:

$$\begin{cases} T_{\mathrm{A}} = T_{\mathrm{a}} \\ T_{\mathrm{B}} = T_{\mathrm{b}} \\ T_{\mathrm{C}} = T_{\mathrm{c}}. \end{cases} \tag{12}$$

Along this route, T_{lag} of $i_{\mathrm{ira1}}/i_{\mathrm{irb1}}/i_{\mathrm{irc1}}$ is redefined as $T_{\mathrm{a\_tr}}/T_{\mathrm{b\_tr}}/T_{\mathrm{c\_tr}}$, whereas T_{lag} of $i_{\mathrm{irA\_T1}}/i_{\mathrm{irB\_T1}}/i_{\mathrm{irC\_T1}}$ is controlled to $T_{\mathrm{a}}/T_{\mathrm{b}}/T_{\mathrm{c}}$. Thereupon, by substituting $T_{\mathrm{a\_tr}}$ and T_{a} for T_{a} and T_{A} in (10), respectively, the setting of $T_{\mathrm{a\_tr}}$ can be obtained, as shown in the following:

$$\begin{cases} T_{\mathrm{a\_tr}} = T_{\mathrm{a}} + [(1 - f_{\mathrm{iir}}/f_{\mathrm{u}})N_{\mathrm{clk}} + 12m_{\mathrm{t}}]/(12f_{\mathrm{iir}}) \\ \text{for positive sequence irregular currents} \\ T_{\mathrm{a\_tr}} = T_{\mathrm{a}} + [(-1 - f_{\mathrm{iir}}/f_{\mathrm{u}})N_{\mathrm{clk}} + 12m_{\mathrm{t}}]/(12f_{\mathrm{iir}}) \\ \text{for negative sequence irregular currents.} \end{cases} \tag{13}$$

For DG2 unit in Fig. 7, the conclusion is entirely the same to DG1 unit. Since DG1 and DG2 units have the same $T_{\mathrm{a\_tr}}/T_{\mathrm{b\_tr}}/T_{\mathrm{c\_tr}}$, $i_{\mathrm{ira1}}/i_{\mathrm{irb1}}/i_{\mathrm{irc1}}$ and $i_{\mathrm{ira2}}/i_{\mathrm{irb2}}/i_{\mathrm{irc2}}$ are in phase. In other words, the irregular currents have been under optimal condition from output by DG units to be injected into the grid.

Regarding the SP system in Fig. 7, by following the analysis mentioned above, a similar conclusion and the setting in the following can be derived:

$$T_{\mathrm{l\_tr}} = T_{\mathrm{l}} + [(1 - f_{\mathrm{iir}}/f_{\mathrm{u}})N_{\mathrm{clk}} + 12m_{\mathrm{t}}]/(12f_{\mathrm{iir}}) \tag{14}$$

where $T_{\mathrm{l\_tr}}$ is the T_{lag} of i_{irs4} and i_{irs5}.

In conclusion, no matter TP transformers or SP transformers, the irregular currents injected into the grid through them are in phase with those injected directly.

If the DG units and their grid-connected transformer are seen as a whole, this whole is just like a DG unit directly connected to the grid under normal conditions [26]. Then, according to the analyses in [26], here for TP irregular currents, the usable f_{iir} are the frequencies that are integer multiples of f_{u} (including negative sequence fundamental frequency), whereas for SP irregular currents, the usable f_{iir} are those in (1b). However, it should be noted that for TP system, normal conditions are difficult to ensure in reality, whereby here the usable f_{iir} have no practical meaning.

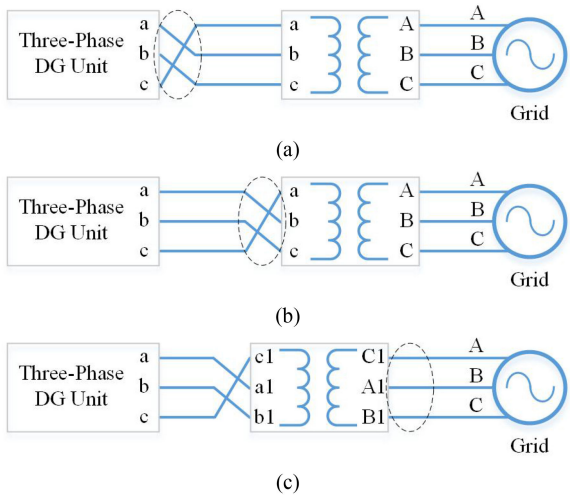

Fig. 8. PSBFs in TP system. (a) Fault at the DG unit output terminal. (b) Fault at the secondary side of a transformer. (c) Fault at the primary side of a transformer.

IV. Constraints on Irregular Currents Under Fault Conditions Considering Compatibility Issues

A. Analysis Based on Phase Symbol Faults (PSBFs) for TP System

PSBFs have been mentioned in [26], which result from wiring errors, as shown in Fig. 8(a). For PSBFs, the phase sequence is correct, and thus they cannot be detected by DG units and do not affect generation. Hence, PSBFs are accepted by commercial inverters. PSBFs mainly occur at the connection points, and we summarize three fault points: DG unit output terminal, primary side, and secondary side of a transformer. Other fault points

or multiple fault points can be equivalent to one of these three points.

In Fig. 8(a), there is a PSBF at the DG unit output terminal. Hereafter, fault points will be marked by dashed boxes. By sorting out the circuits, the fault point is equivalently transferred to the secondary side of the transformer, as shown in Fig. 8(b). For a transformer, if both its primary and secondary phase symbols change in the same direction, e.g., A–B–C to B–C–A and a–b–c to b–c–a, its parameters (including winding connection symbol) will not change. In this case, Fig. 8(b) can be transformed to Fig. 8(c), where the changed phase symbols are renamed to A1, B1, C1 and a1, b1, c1. Hence, the fault point is equivalently transferred to the primary side. In fact, by analyzing all the cases of PSBFs, it is found that wherever a PSBF is, it can be equivalent to a fault at the primary side of the transformer.

As mentioned in [26], actually, DG units cannot detect a PSBF, wherever the fault is. Consequently, $T_{\mathrm{a\_tr}}$ can only be set by the nominal N_{clk} of the transformer in accordance with (13), and here $T_{\mathrm{a\_tr}}$ is specifically defined as $T_{\mathrm{a\_tr\_nom}}$. However, after the primary and secondary phase symbols change, e.g., that shown in Fig. 8(c), if N_{clk} also changes despite not in Fig. 8(c), $T_{\mathrm{a\_tr}}$ actually should be set according to the changed N_{clk}, which is defined as $T_{\mathrm{a\_tr\_flt}}$. If $T_{\mathrm{a\_tr\_flt}} \neq T_{\mathrm{a\_tr\_nom}}$, T_{lag} of the primary irregular currents injected into the grid cannot be controlled as expected, whereby the irregular currents may still cancel each other out. Consequently, whether N_{clk} will change should be paid special attention after phase symbols change.

Since any PSBF can be equivalent to a fault at the primary side of the transformer, which infers that N_{clk} will not change after phase symbols change, it is always true that $T_{\mathrm{a\_tr\_flt}} = T_{\mathrm{a\_tr\_nom}}$ and T_{lag} of the primary irregular currents can be controlled as expected. For the case in Fig. 8(c), T_{lag} of irregular current of phase A1 must be T_{a}, i.e., the expected result.

If several DG units share a transformer, as shown in Fig. 7, they can be equivalently resolved into several parallel parts in which a transformer connects only one DG unit according to superposition theorem. For every part, if there is a PSBF, this fault can be equivalently transferred to the primary side of the transformer, like Fig. 8(c). Then, if every part is seen as a whole, like a DG unit, the situation is just like DG units under direct couple conditions mentioned in [26]. According to the conclusions in [26], the usable f_{iir} here are those in (1a).

In summary, for TP DG units equipped with grid-connected transformers, considering PSBFs, $T_{\mathrm{a\_tr}}$ should be set as (13), where N_{clk} is the nominal clock position of the transformer, and f_{iir} should be selected from (1a). By means of this measure, from the conclusion mentioned in Section I-E, T_{lag} of the primary irregular currents of a TP transformer will be T_{a} (i.e., $T_{\mathrm{a}} = T_{\mathrm{b}} = T_{\mathrm{c}}$), whereas T_{lag} of TP irregular currents directly injected (see the DG3 unit in Fig. 7) is also T_{a}. Therefore, the irregular currents injected into the grid through transformers and those directly injected will be in phase.

B. Analysis Based on PSBFs for SP System

Unlike direct couple conditions, under conditions with grid-connected transformers, SP DG units are not coupled to live wires and neutral wires of the grid, whereby they cannot sense PSBFs any longer and these faults may exist in a SP system [26]. Likewise, there are also three fault points regarding PSBFs, as shown in Fig. 9.

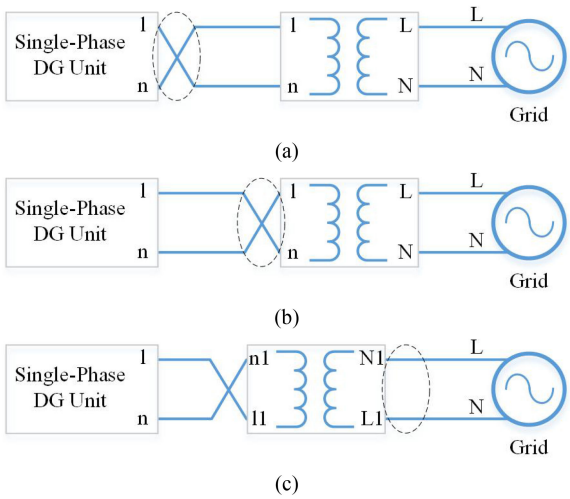

Fig. 9. PSBFs in SP system. (a) Fault at the DG unit output terminal. (b) Fault at the secondary side of a transformer. (c) Fault at the primary side of a transformer.

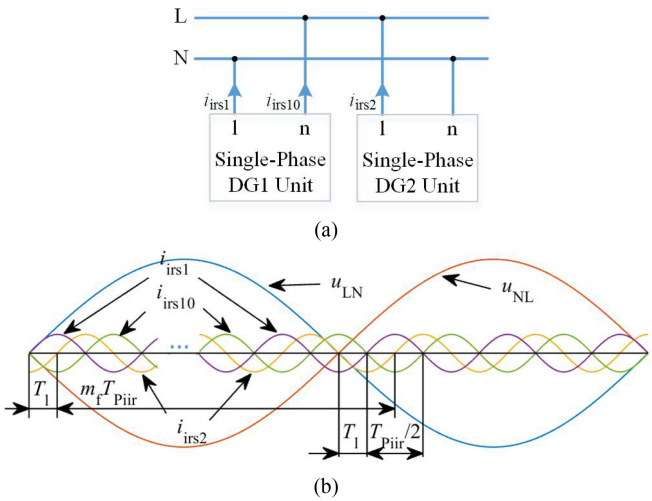

Fig. 10. SP DG unit with a PSBF. (a) Faulty line. (b) Irregular currents injection.

By following the analysis before, all PSBFs can still be equivalent to a fault at the primary side of the transformer, and $T_{\mathrm{l\_tr\_flt}} = T_{\mathrm{l\_tr\_nom}}$, where the definitions of $T_{\mathrm{l\_tr\_flt}}$ and $T_{\mathrm{l\_tr\_nom}}$ are similar to those of $T_{\mathrm{a\_tr\_flt}}$ and $T_{\mathrm{a\_tr\_nom}}$, respectively. The DG unit and transformer can still be seen as a whole, which is represented by a new DG unit, i.e., the DG1 unit in Fig. 10(a).

In Fig. 10(a), the PSBF in DG1 unit causes the reference voltage (i.e., terminal voltage u_{ln}) of i_{irs1} to be u_{NL} rather than u_{LN}. Thereupon, the irregular currents injection is shown in Fig. 10(b), where m_{f} is a positive integer.

According to the compatibility requirement, the phase difference between i_{irs10} and i_{irs2} should be in $[-\pi/2, \pi/2]$. Since $\pi/2$ corresponds to the time of $T_{\mathrm{Piir}}/4$, the following relationship

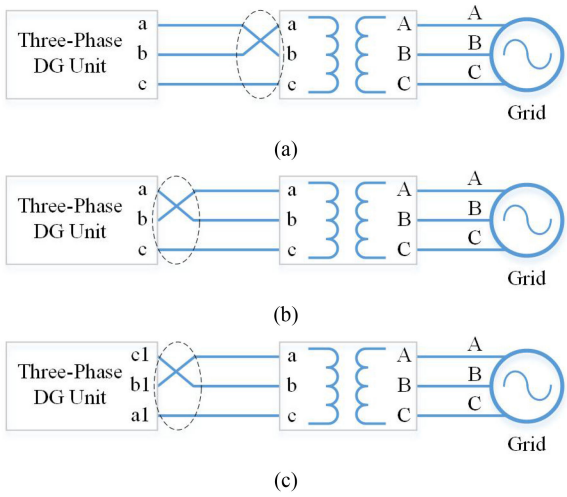

Fig. 11. PSQFs in TP system (relating to the secondary side of a transformer). (a) PSQF at the secondary side of a transformer. (b) PSQF at the DG unit output terminal. (c) PSBF at the DG unit output terminal.

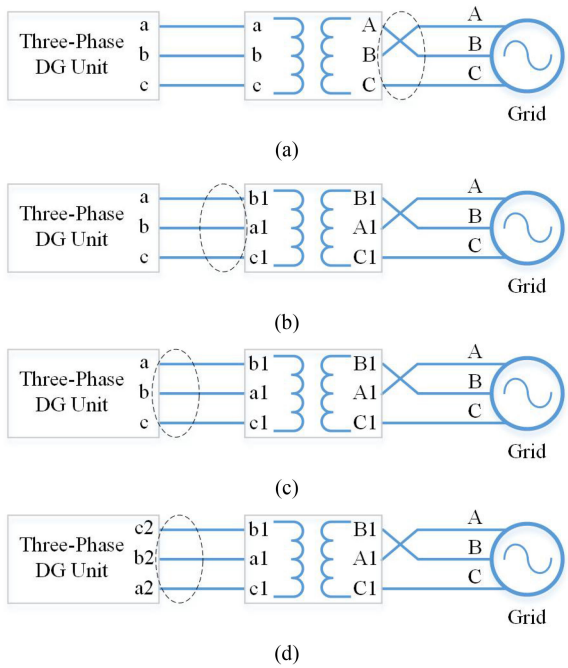

Fig. 12. PSQFs in TP system (relating to the primary side of a transformer). (a) PSQF at the primary side of a transformer. (b) PSQF at the secondary side of a transformer. (c) PSQF at the DG unit output terminal. (d) PSBF at the DG unit output terminal.

should be met from Fig. 10(b):

$$-T_{\mathrm{Piir}}/4 \le T_{\mathrm{Pu}}/2 + T_{\mathrm{l}} + T_{\mathrm{Piir}}/2 - T_{\mathrm{l}} - m_{\mathrm{f}}T_{\mathrm{Piir}} \le T_{\mathrm{Piir}}/4.$$

According to the analyses in [26], under any condition, f_{iir} must be an integer multiple of f_{u}, which is a basic requirement. Therefore, the following equation can be derived from the above relationship, where m_{f} is a positive integer greater than 1:

$$f_{\mathrm{iir}} = (2m_{\mathrm{f}} - 1)f_{\mathrm{u}}.$$

By using the above equation to check, it can be found that the irregular currents injected into the grid through transformers and those directly injected [e.g., i_{irs10} and i_{irs2} in Fig. 10(a)] will be in phase. In other words, in terms of irregular current injection, the DG units with faults and those without faults are exactly the same. Furthermore, according to the conclusions in [26], in order for the irregular current injection methods in SP DG units and TP DG units to be compatible with each other, (1b) should be met. Accordingly, the final usable f_{iir} are the intersection of (1b) and the above equation, as shown in the following:

$$f_{\mathrm{iir}} = (6q \pm 1)f_{\mathrm{u}}. \tag{15}$$

In conclusion, considering PSBFs in the SP system, $T_{\mathrm{l\_tr}}$ should be set as (14), where N_{clk} is the nominal clock position of the transformer, and f_{iir} should be selected from (15). Afterward, there is still the optimal condition that the irregular currents injected into the grid through transformers and those directly injected are in phase.

C. Analysis Based on Phase Sequence Faults (PSQFs) for TP System

In this article, a PSQF is defined as the condition where the phase sequences of a terminal and the connected cables mismatch each other. The fault points are the same as those of PSBFs. For example, Fig. 11(a) shows a PSQF at the secondary side of a transformer.

1) Faults at DG Unit Output Terminals or Secondary Sides of Transformers: As shown in Fig. 11(a), the PSQF at the secondary side of the transformer can be equivalently transferred to the DG unit output terminal, as shown in Fig. 11(b). As mentioned in [26], the DG unit can detect and translate the PSQF into a PSBF by adjusting its inner phase sequence to not affect generation, as shown in Fig. 11(c). Hence, PSQFs are generally tolerated by commercial inverters to avoid wiring correction and the resultant time and labor costs.

By analyzing all the cases of such faults, we find that all these faults, which are at both DG unit output terminals and secondary sides of transformers, can be equivalently translated into a PSBF at the DG unit output terminal, like in Fig. 11(c). Accordingly, these faults can be dealt with by referring to the PSBFs discussed in Section IV-A.

2) Faults at Primary Sides of Transformers: Such a fault is shown in Fig. 12(a). As above, by changing the phase symbols on both sides of the transformer synchronously, the PSQF is transferred to the secondary side of the transformer, as shown in Fig. 12(b), where the positive phase sequence of the transformer terminal is from bottom to top rather than the normal sequence from top to bottom. Since PSQFs at secondary sides of transformers can be seen as PSBFs at the DG units output terminals, as concluded above, if the fault transfer of Fig. 12(a) to (b) is equivalent, the PSQF at the primary side of the transformer can also be seen as the PSBF at the DG unit output terminal, as shown in Fig. 12(d); actually, any case of such faults is like this.

A fault transfer like Fig. 12(a) to (b) is equivalent if the winding connection symbol (actually N_{clk}) has not changed after

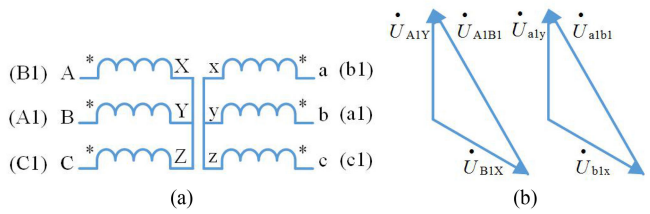

Fig. 13. Phase symbols change (nominal Y,y0 connection). (a) Transformer with Y,y0 connection. (b) Voltages phasor diagram after the phase symbols change.

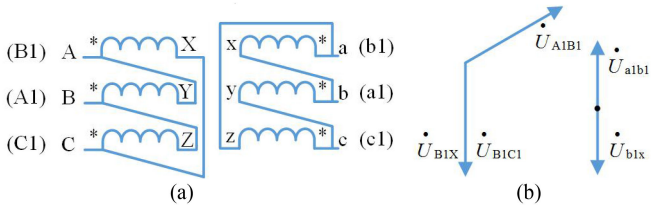

Fig. 14. Phase symbols change (nominal D,d2 connection). (a) Transformer with D,d2 connection. (b) Voltages phasor diagram after the phase symbols change.

the phase symbols change. The following will discuss the change of N_{clk}.

Before the discussing, a property of the usable f_{iir} here will be introduced.

As mentioned in Section IV-C1, PSQFs at both secondary sides of transformers and DG unit output terminals should be dealt with by following PSBFs at DG unit output terminals, whereby f_{iir} should meet (1a). On the other hand, DG units can discern PSQFs, but cannot locate them. Thus, for PSQFs, the final usable f_{iir} must be the intersection of (1a) and the usable frequencies based on the PSQFs at primary sides of transformers. In other words, the final usable f_{iir} must meet (1a). For ease of analysis, the following will only discuss f_{iir} determined by (1a).

According to the analysis of all kinds of winding connections, it is found that for the transformers with connections of Y,y or D,d, after a phase symbols change like Fig. 12(a) to (b), N_{clk} of some connections will not change while the others will. Nonetheless, considering the above conclusion that f_{iir} should meet (1a), for all connections of Y,y and D,d, there are always $T_{\mathrm{a\_tr\_flt}} = T_{\mathrm{a\_tr\_nom}}$, which will be demonstrated later. Therefore, in terms of the irregular current injection studied here, if the connection of a transformer is Y,y or D,d, the PSQF at the primary side can be equivalently transferred to the secondary side [e.g., Fig. 12(a) to (b)].

As regards the transformers with connections of Y,d or D,y, after the mentioned phase symbols change, N_{clk} will change and there is $T_{\mathrm{a\_tr\_flt}} \neq T_{\mathrm{a\_tr\_nom}}$, which means that the PSQF at the primary side cannot be equivalently transferred to the secondary side.

The following will demonstrate three examples of phase symbols change.

Fig. 13 illustrates a transformer with Y,y0 connection and its voltages phasor diagram. It can be seen that despite the PSQF, the connection is still Y,y0 after the phase symbols change.

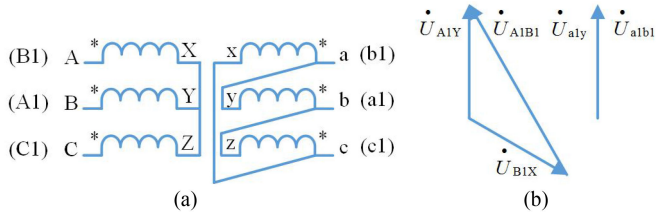

Fig. 15. Phase symbols change (nominal Y,d11 connection). (a) Transformer with Y,d11 connection. (b) Voltages phasor diagram after the phase symbols change.

Fig. 14 illustrates a transformer with D,d2 connection and its voltages phasor diagram. Fig. 14(b) shows that the connection becomes D,d10 after the phase symbols change.

According to (13), if positive sequence irregular currents are output, $T_{\mathrm{a\_tr\_nom}}$ and $T_{\mathrm{a\_tr\_flt}}$ can be calculated as shown in the following:

$$T_{\mathrm{a\_tr\_nom}} = T_{\mathrm{a}} + [2(1 - f_{\mathrm{iir}}/f_{\mathrm{u}}) + 12m_{\mathrm{t\_nom}}]/(12f_{\mathrm{iir}})$$

$$T_{\mathrm{a\_tr\_flt}} = T_{\mathrm{a}} + [10(1 - f_{\mathrm{iir}}/f_{\mathrm{u}}) + 12m_{\mathrm{t\_flt}}]/(12f_{\mathrm{iir}})$$

where $m_{\mathrm{t\_nom}}$ and $m_{\mathrm{t\_flt}}$ are the m_{t} corresponding to $T_{\mathrm{a\_tr\_nom}}$ and $T_{\mathrm{a\_tr\_flt}}$, respectively. Considering f_{iir} should meet (1a) and $f_{\mathrm{iir}} = 1/T_{\mathrm{Piir}}$, the above equations can be simplified into the following equations:

$$T_{\mathrm{a\_tr\_nom}} = T_{\mathrm{a}} - qT_{\mathrm{Piir}}/2 + m_{\mathrm{t\_nom}}T_{\mathrm{Piir}} \tag{16a}$$

$$T_{\mathrm{a\_tr\_flt}} = T_{\mathrm{a}} - qT_{\mathrm{Piir}}/2 + (m_{\mathrm{t\_flt}} - 2q)T_{\mathrm{Piir}}. \tag{16b}$$

According to the definition of T_{lag}, there are $0 \leq T_{\mathrm{a\_tr\_nom}} < T_{\mathrm{Piir}}$ and $0 \leq T_{\mathrm{a\_tr\_flt}} < T_{\mathrm{Piir}}$, whereby the following inequality is true:

$$-T_{\mathrm{Piir}} < T_{\mathrm{a\_tr\_nom}} - T_{\mathrm{a\_tr\_flt}} < T_{\mathrm{Piir}}.$$

By substituting (16a) and (16b) into the above inequality, the following inequality can be obtained:

$$-1 < m_{\mathrm{t\_nom}} - (m_{\mathrm{t\_flt}} - 2q) < 1.$$

Since $m_{\mathrm{t\_nom}}$, $m_{\mathrm{t\_flt}}$, and q are all integers, there must be the following relationship:

$$m_{\mathrm{t\_nom}} = m_{\mathrm{t\_flt}} - 2q.$$

From (16a), (16b), and the above relationship, there is

$$T_{\mathrm{a\_tr\_nom}} = T_{\mathrm{a\_tr\_flt}}.$$

This means that although $T_{\mathrm{a\_tr}}$ can only be set by means of the nominal N_{clk} and N_{clk} has changed after the phase symbols change, expected results will still be achieved. As for negative sequence currents, the same conclusion can be reached.

Fig. 15 illustrates a transformer with Y,d11 connection and its voltages phasor diagram. Fig. 15(b) shows that after the phase symbols change, the connection becomes Y,d1, and there is $T_{\mathrm{a\_tr\_flt}} \neq T_{\mathrm{a\_tr\_nom}}$ according to (13). Therefore, since $T_{\mathrm{a\_tr}}$ will always be set to $T_{\mathrm{a\_tr\_nom}}$, T_{lag} of the primary irregular currents will not be as expected in this case.

So, how to deal with the problem of clock position change like that in Fig. 15 regarding irregular current injection?

First of all, a characteristic of $T_{\rm lag}$ should be explained again.

According to the relationship between $T_{\rm a}$, $T_{\rm b}$, and $T_{\rm c}$ derived in [26], which are actually universal formulas, it can be calculated that when $f_{\rm iir}$ meets (1a), the TP irregular currents of a terminal will have the same $T_{\rm lag}$, i.e., just the conclusion mentioned in Section I-E. Since for PSQFs, $f_{\rm iir}$ should meet (1a), which has mentioned above, there are $T_{\rm a} = T_{\rm b} = T_{\rm c}$, $T_{\rm a\_tr} = T_{\rm b\_tr} = T_{\rm c\_tr}$, and $T_{\rm A} = T_{\rm B} = T_{\rm C}$, whereby $T_{\rm a}$, $T_{\rm a\_tr}$, and $T_{\rm A}$ can be used to represent $T_{\rm lag}$ of the irregular currents. The following will discuss the problem of clock position change.

Here, we take positive sequence irregular currents for example, and designate $N_{\rm clk0}$ as the nominal clock position while $N_{\rm clk1}$ as the changed clock position. The following equation can be obtained from (13):

$$T_{\rm a\_tr\_nom} = T_{\rm a} + [(1 - f_{\rm iir}/f_{\rm u})N_{\rm clk0} + 12m_{\rm t0}]/(12f_{\rm iir})$$

where $m_{\rm t0}$ denotes the $m_{\rm t}$ corresponding to $N_{\rm clk0}$. If $T_{\rm a\_tr}$ is still set to $T_{\rm a\_tr\_nom}$ when the clock position has become $N_{\rm clk1}$, $T_{\rm lag}$ of the primary irregular currents of the transformer, defined as $T_{\rm A1}$, can be obtained by substituting the above $T_{\rm a\_tr\_nom}$ for $T_{\rm a}$ in (10), as shown in the following:

$$T_{\rm A1} = T_{\rm a} + [(1 - f_{\rm iir}/f_{\rm u})(N_{\rm clk0} - N_{\rm clk1}) + 12(m_{\rm t0} - m_{\rm t1})]/(12f_{\rm iir}) \tag{17}$$

where $m_{\rm t1}$ denotes $m_{\rm t}$ corresponding to $N_{\rm clk1}$.

By far, all obtained conclusions based on conditions with grid-connected transformers and the conclusions based on direct couple conditions obtained in [26] show that for TP irregular currents $f_{\rm iir}$ should be selected from (1a), and the irregular currents injected into the grid are always in phase, which infers that their $T_{\rm lag}$ is always $T_{\rm a}$. Thus, according to the compatibility requirement and by following the analysis in [26], the following relationship should be satisfied:

$$-T_{\rm Piir}/4 \le T_{\rm A1} + T_{\rm int} - T_{\rm a} \le T_{\rm Piir}/4$$

where $T_{\rm int}$ can be one of 0, -$T_{\rm Piir}$, and $T_{\rm Piir}$ [26]. By combining the above relationship and (17), the following equation can be derived:

$$-T_{\rm Piir}/4 \le [(1 - f_{\rm iir}/f_{\rm u})(N_{\rm clk0} - N_{\rm clk1}) + 12(m_{\rm t0} - m_{\rm t1})]/(12f_{\rm iir}) + T_{\rm int} \le T_{\rm Piir}/4. \tag{18}$$

The following inequality can be obtained by taking the related $N_{\rm clk}$ of the transformer in Fig. 15:

$$(-1/2 + 6m_{\rm t10})f_{\rm u} \le f_{\rm iir} \le (5/2 + 6m_{\rm t10})f_{\rm u}$$

where $m_{\rm t10}$ is an integer. Considering $f_{\rm iir}$ should satisfy (1a), for positive sequence irregular currents, $f_{\rm iir}$ can only be selected from the following equation:

$$f_{\rm iir} = (6q + 1)f_{\rm u}. \tag{19}$$

This equation can be validated by substituting it into (18). For the example in Fig. 15, by substituting (19) into (17), the following relationship can be obtained:

$$T_{\rm A1} = T_{\rm a}. \tag{20}$$

This relationship shows that the irregular currents injected into the grid through the transformer in Fig. 15(a) will be in phase with those directly injected.

Although (19) and (20) are derived from the example in Fig. 15, through analyzing the other cases of PSQFs at primary sides of the transformers with connections of Y,d or D,y, it is found that $f_{\rm iir}$ should still be selected in accordance with (19), and (20) is still true.

With regard to negative sequence irregular currents, by following the above analysis, (20) and an equation similar to (19) are also derived. In summary, the final usable $f_{\rm iir}$ are shown in the following:

$$\begin{cases} f_{\rm iir} = (6q + 1)f_{\rm u}, \text{ for positive sequence irregular currents} \\ f_{\rm iir} = (6q - 1)f_{\rm u}, \text{ for negative sequence irregular currents.} \end{cases} \tag{21}$$

These equations reveal that PSQFs at primary sides of the transformers with Y,d or D,y connections further constrain the selection of $f_{\rm iir}$.

In conclusion, for PSQFs at primary sides of transformers, if the transformer connection is Y,y or D,d, the faults can be dealt with like PSBFs discussed in Section IV-A, and if the transformer connection is Y,d or D,y, $T_{\rm a\_tr}$ should be set as (13), where $N_{\rm clk}$ is the nominal clock position of the transformer, and $f_{\rm iir}$ should be selected from (21).

In any case, according to the previous conclusions, as long as the corresponding solution is implemented, the injected irregular currents under conditions with grid-connected transformers and those under direct couple conditions are in phase, whereby any two clusters of irregular currents injected through two transformers should also be in phase.

By integrating the conclusions achieved above and those in [26], the usable frequencies are shown in Table I. It must be noted that in TP system, DG units can perceive PSQFs but not PSBFs, and can know the winding connections of transformers in advance [26]. Therefore, there may be PSBFs even if DG units detect no fault, and then the final usable $f_{\rm iir}$ should be the intersection of the usable frequencies based on normal conditions and those based on PSBFs. Additionally, after DG units adjust their inner phase sequences under PSQFs, the irregular current injection is based on the adjusted phase symbols, e.g., a1–b1–c1 in Fig. 11(c). Considering the frequencies of TP irregular currents in Table I satisfy (1a), the corresponding TP irregular currents of a terminal will always have the same $T_{\rm lag}$.

The analysis later will indicate that $f_{\rm iir}$ is best as low as possible. Throughout the lowest usable frequencies in Table I, in TP system, negative sequence irregular currents are more suitable as injected currents due to their lower available frequencies, and the transformers with connections of Y,y or D,d are recommended.

V. Further Discussion on Actual Transformers and Final Complete Solution to Compatibility Issues

The previous conclusions are based on ideal transformers, whereas, for actual transformers, the leakage impedance may bring some variations to the results before. As shown in Fig. 16(a), it is a simplified circuit of a phase of an actual transformer. The voltages phasor diagram is presented in Fig. 16(b).

TABLE I
USABLE FREQUENCY ORDERS FOR IRREGULAR CURRENTS

	No transformer	Equipped with transformers		
		Three-phase system: able to ensure no phase sequence fault at the primary sides, or the transformers with connections of Y,y or D,d	Three-phase system: unable to ensure no phase sequence fault at the primary sides, and the transformers with connections of Y,d or D,y	Setting of T_{a_tr} and T_{l_tr}
		Single-phase system: able to ensure no phase symbol fault	Single-phase system: unable to ensure no phase symbol fault	
Three-phase positive sequence currents	$3q$+1	$3q$+1	$6q$+1	Referring to (13)
Three-phase negative sequence currents	$3q$ - 1	$3q$ - 1	$6q$ - 1	
Single-phase currents	$3q$±1	$3q$±1	$6q$±1	Referring to (14)

where q is a positive integer and N_{clk} is the nominal clock position of the transformer.

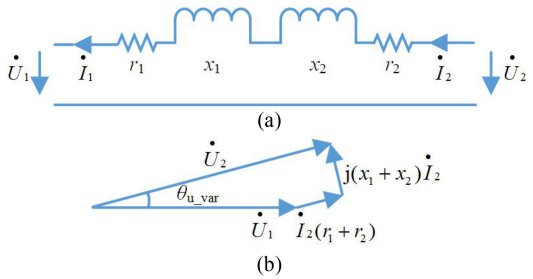

Fig. 16. Analysis of a phase of an actual transformer. (a) Simplified circuit of a phase of an actual transformer. (b) Phase difference between $\dot{U}_1$ and $\dot{U}_2$ under a condition that the DG unit is based on unity power factor control.

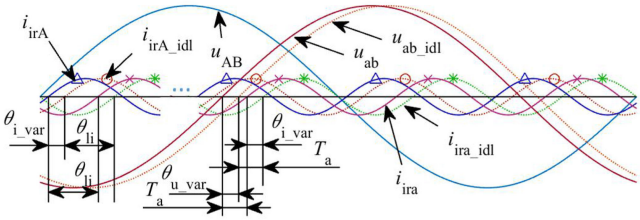

Fig. 17. Phase variations in an actual transformer.

Fig. 16(b) shows a common scenario where the DG unit is based on unity power factor control, i.e., $\dot{U}_2$ being in phase with $\dot{I}_2$. It demonstrates that $\dot{U}_2$ leads $\dot{U}_1$ by θ_{u_var}, whereas for an ideal transformer, $\dot{U}_2$ is in phase with $\dot{U}_1$, and as a primary voltage, $\dot{U}_1$ can be seen as a constant. Thus, the actual secondary phase voltage leads the ideal one by θ_{u_var}, and thereby the same is true of the secondary line voltage while the leading angle is also θ_{u_var}. Accordingly, for an actual transformer, Fig. 4 can be redrawn as Fig. 17 where u_{ab_idl}, i_{ira_idl}, and i_{irA_idl} represent the ideal line voltage and line currents. In Fig. 17, since u_{ab} leads u_{ab_idl}, i_{ira} will lead i_{irA_idl} accordingly, and the leading angle is noted as θ_{i_var}.

On the other hand, as shown in Fig. 16(a), $\dot{I}_1$ is equal to $\dot{I}_2$, which is the same as that in an ideal transformer. Thus, considering for ideal and actual transformers, the phasor relationships between the phase currents and the line currents are the same, the phase differences between the primary and secondary line currents, i.e., θ_{li}, are also the same for two such transformers. Accordingly, i_{irA} will also lead i_{irA_idl} by θ_{i_var}, like i_{ira} to i_{irA_idl}, as shown in Fig. 17. Since i_{irA} and i_{irA_idl} have the same reference voltage, i.e., u_{AB}, there must be a difference of θ_{i_var} between the actual T_A and the ideal one. In other words, the actual T_A (including T_L in single system) may be unable to be controlled to the expected T_a (T_l) even if Table I is obeyed. Although θ_{i_var} is generally small and may not damage the compatibility, it deprives the optimal condition [i.e., (12)] after all. Thus, a smaller θ_{i_var} is expected. The time corresponding to θ_{i_var} and θ_{u_var} is $T_{Piir}\theta_{i\_var}/(2\pi)$ and $T_{Pu}\theta_{u\_var}/(2\pi)$, respectively. Fig. 17 clearly shows the following relationship:

$$T_a - T_{Piir}\theta_{i\_var}/(2\pi) = T_a - T_{Pu}\theta_{u\_var}/(2\pi).$$

The above equation can be simplified as

$$\theta_{i\_var} = \theta_{u\_var} f_{iir}/f_u.$$

The equation above indicates that to make θ_{i_var} smaller, f_{iir} based on Table I should be as small as possible (e.g., let $q = 1$).

In addition, if possible, the primary voltages of transformers are suggested to be measured instead of the secondary voltages, and then the ideal secondary voltages can be calculated and used as the reference voltages, whereby θ_{i_var} will be zero and the adverse effect resulting from leakage impedance will be avoided.

To sum up, a complete solution to compatibility issues with irregular current injection methods in multi-DG units (including those equipped with or without grid-connected transformers) can be generalized into the following three points.

1) Reference the terminal voltages of DG units to conduct irregular current injection, and the injection pattern is shown in Fig. 2.
2) T_{lag} of irregular currents is set as T_a (in TP system) or T_l (in SP system) under direct couple conditions and set as T_{a_tr} or T_{l_tr} under conditions with grid-connected transformers.
3) For T_a and T_l, we suggest the following setting mentioned in [26]:

$$\begin{cases} T_a = T_{Pu}/12 \\ T_l = 0. \end{cases} \tag{22}$$

4) Select irregular current frequencies and set T_{a_tr} and T_{l_tr} according to Table I, and the selected frequencies should be as small as possible.

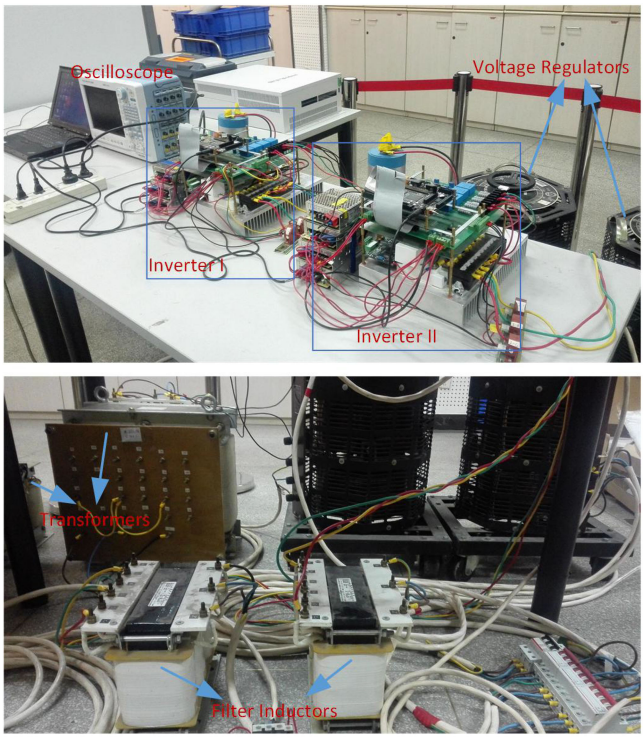

Fig. 18. Schematic diagram of the experimental setups.

TABLE II
SPECIFICATIONS OF THE EXPERIMENTAL INVERTERS

Inverter I/II power rating	10 kW
Inverter topology	Three-phase output and single-stage with DC-link
IGBT specification	1200 V/50 A
Switch frequency	10 kHz
DC-link voltage	382 V
Filter I/II ($L_{\rm f}$)	5 mH
Interconnection voltage	380 V/50 Hz

The implementation of irregular current injection based on inverters and other related notable factors have been mentioned in [26], which are still applicable in this article.

VI. Validations by Experiments and Simulations

In this section, (22) is adopted and the frequencies selected from Table I will be as small as possible. All cases in this section are based on ordinary generation mode, which means that the irregular currents should be extracted from the measured currents.

The experimental setups are shown in Fig. 18. There are two independent inverters equipped with grid-connected transformers. The dc source of each inverter is supplied by a TP rectifier (integrated in the inverter) whose ac source is from a voltage regulator. The input terminals of the voltage regulators are connected to the grid.

The specifications of the experimental inverters are shown in Table II.

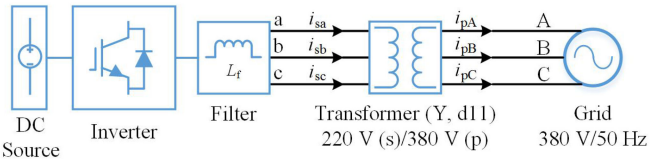

Fig. 19. Test circuit regarding the setting of $T_{\rm a\_tr}$.

A. Experimental Validation Regarding the Setting of $T_{\rm a\_tr}$

The circuit shown in Fig. 19 is used to validate the setting of $T_{\rm a\_tr}$. In this experiment, the inverter outputs negative sequence 100 Hz currents of 1 A (amplitude).

According to (13), $T_{\rm a\_tr}$ is set to $5T_{\rm Pu}/24$. The experimental results are shown in Fig. 20. In the upper right zone, it can be seen that $T_{\rm A}$ has been controlled to the expected value $T_{\rm Pu}/12$, i.e., $T_{\rm a}$. Thus, these results verify the accuracy of (13), i.e., the setting of $T_{\rm a\_tr}$.

B. Validations Regarding TP System

1) Experimental Test Based on Normal Conditions: The experimental circuit is shown in Fig. 21, where both inverters are based on unity power factor control.

Here, negative sequence 100 Hz currents are selected as the injected currents whose frequency is the lowest one from Table I. The experimental results are shown in Fig. 22. Obviously, $T_{\rm lag}$ of both $i_{\rm ir\_1A}$ and $i_{\rm ir\_2A}$, symbolized by the horizontal bold solid line in the upper right zone, are $T_{\rm a}$, which means that $i_{\rm ir\_1A}$ and $i_{\rm ir\_2A}$ will be in phase whenever they are injected. Therefore, $i_{\rm ir\_aggA}$ rises after $i_{\rm ir\_2A}$ is injected, whereby such irregular current is usable under normal conditions.

2) Experimental Test Based on a PSBF: The experimental circuit is shown in Fig. 23, where there is a PSBF at the primary side of transformer I. To follow the above experimental route, negative sequence 100 Hz currents are still employed, whereas the other conditions except the circuit remain unchanged.

As shown in Fig. 23, based on the PSBF, $i_{\rm ir\_1A}$ is output from the nominal terminal C of transformer I and converges with $i_{\rm ir\_2A}$ on phase A of the grid. Therefore, although the actually reference voltage of both the irregular currents is $u_{\rm AB}$ of the grid, $T_{\rm lag}$ of $i_{\rm ir\_1A}$ and $i_{\rm ir\_2A}$ is controlled to $T_{\rm c}$ and $T_{\rm a}$, respectively. The experimental results are shown in Fig. 24.

However, it has been concluded that $f_{\rm iir}$ (e.g., the 100 Hz here) from Table I must lead to $T_{\rm a} = T_{\rm b} = T_{\rm c}$. This point has been clearly illustrated in the upper right zone of Fig. 24. Thereby, $i_{\rm ir\_1A}$ and $i_{\rm ir\_2A}$ are in phase, and $i_{\rm ir\_aggA}$ increases after $i_{\rm ir\_2A}$ is injected. Such irregular current is usable under the PSBF accordingly.

3) Simulation Test Based on a PSQF: The simulations are based on the circuit in Fig. 25. In this case, to start with, we still test negative sequence 100 Hz currents. For comparison, two transformers with Y,y0 and D,y11 connections are successively tested. The simulation results are shown in Fig. 26, where $i_{\rm ir\_noTrsf}$ and $i_{\rm ir\_Yy0\_flt}$/$i_{\rm ir\_Dy11\_flt}$ denote the irregular currents output from inverter I and the primary side of the transformer, respectively.

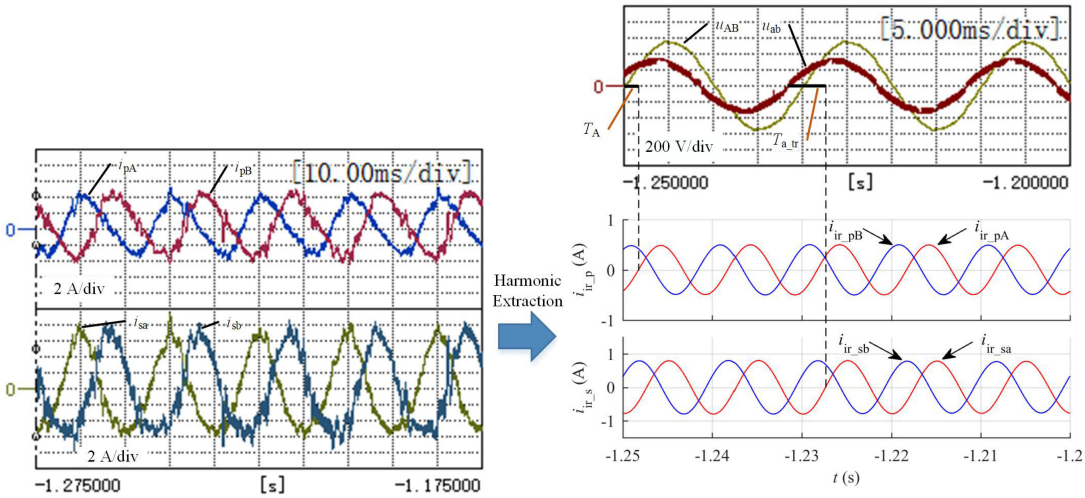

Fig. 20. Validation of the setting of $T_{\mathrm{a\_tr}}$ (the subscripts p and s denote the primary and secondary sides, respectively; A, B, a, and b are the phase symbols; and ir represents irregular currents).

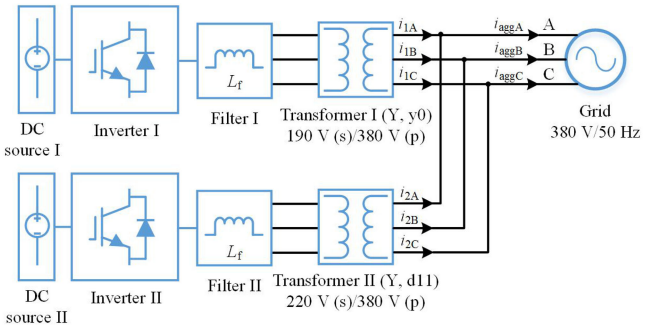

Fig. 21. Test circuit based on normal conditions.

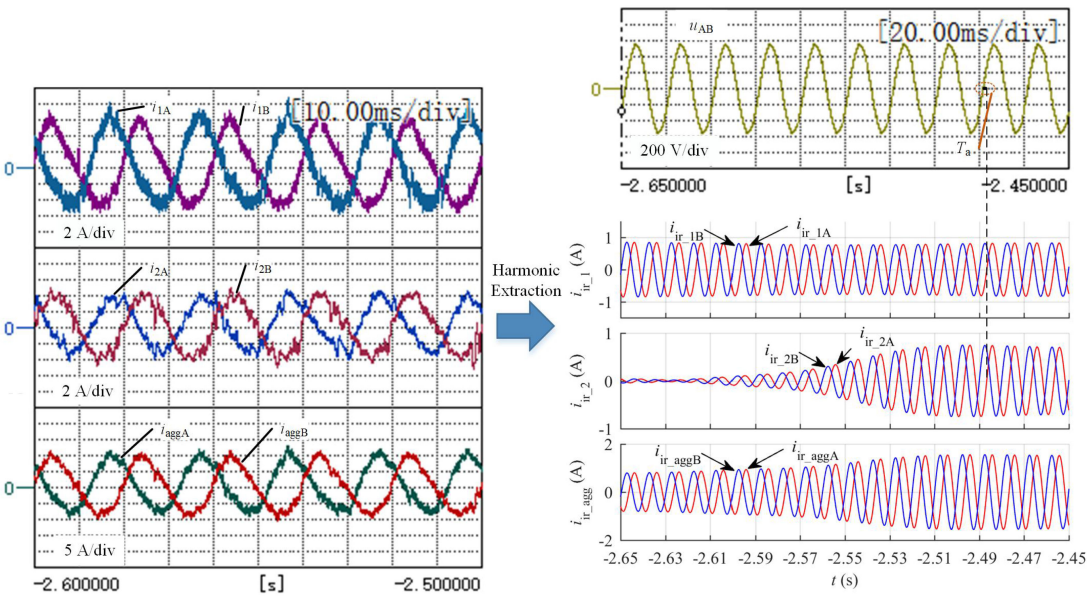

Fig. 22. Waveforms before and after the injection of negative sequence 100 Hz currents from inverter II (based on normal conditions).

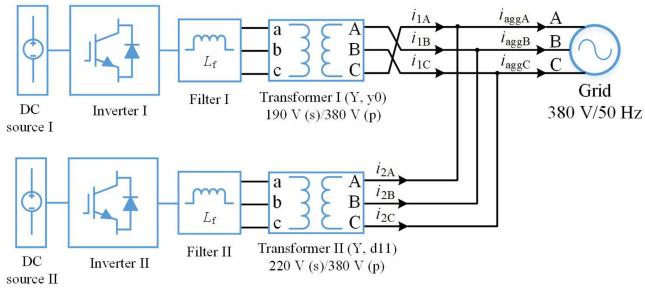

Fig. 23. Test circuit with a PSBF.

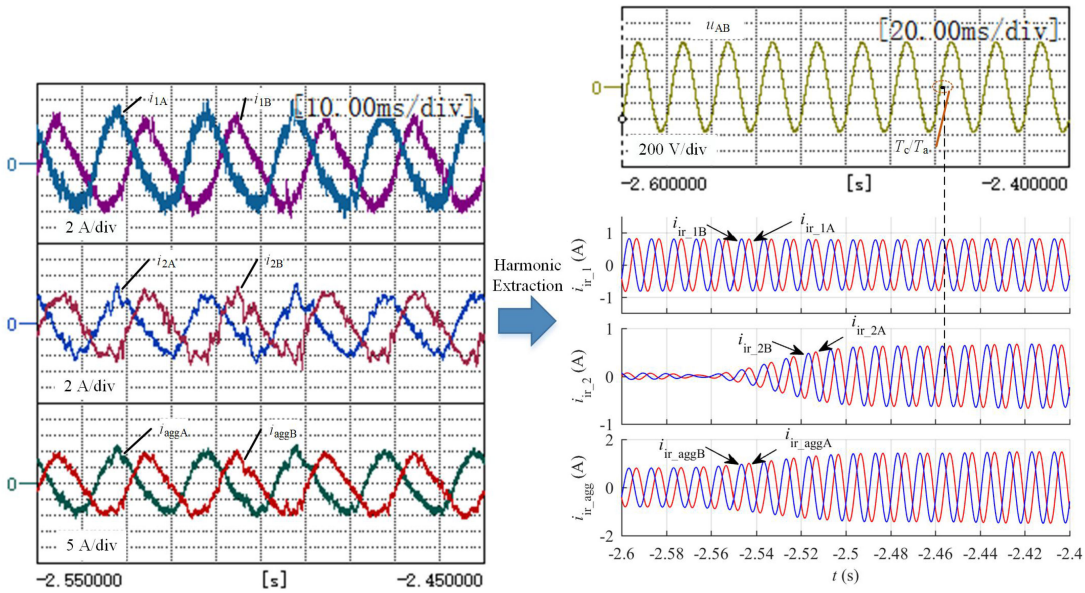

Fig. 24. Waveforms before and after the injection of negative sequence 100 Hz currents from inverter II (based on a PSBF).

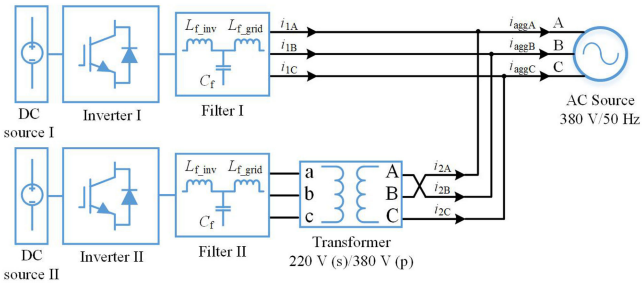

Fig. 25. Simulation circuit with a PSQF.

In Fig. 26(a), when the transformer connection is Y,y0, $T_{\rm lag}$ of all the irregular currents is controlled to $T_{\rm a}$, and $i_{\rm ir\_2A}$, $i_{\rm ir\_2B}$ and $i_{\rm ir\_2C}$ are in phase with $i_{\rm ir\_1A}$, $i_{\rm ir\_1B}$ and $i_{\rm ir\_1C}$, respectively, whereas, in Fig. 26(b), when the transformer connection is D,y11, $i_{\rm ir\_2A}$, $i_{\rm ir\_2B}$, and $i_{\rm ir\_2C}$ are almost out of phase with $i_{\rm ir\_1A}$, $i_{\rm ir\_1B}$ and $i_{\rm ir\_1C}$, respectively, whereby these two clusters of irregular currents must cancel each other out after their convergence. Consequently, when equipped with a transformer with D,y11 connection, the inverter should not adopt negative sequence 100 Hz currents in case of PSQFs; however, for a transformer with Y,y0 connection, this irregular current is usable.

Overall, it can be seen that although negative sequence 100 Hz currents are universal under both the normal and PSBF conditions, they are unusable under the PSQF. In view of this, another irregular current based on Table I, negative sequence 250 Hz currents will be tested below, which are expected to be universal under the PSQF. The test procedure is the same as above, and the simulation results are shown in Fig. 27.

Fig. 27 shows that whether the transformer connection is Y,y0 or D,y11, $i_{\rm ir\_2A}$, $i_{\rm ir\_2B}$, and $i_{\rm ir\_2C}$ are always in phase with $i_{\rm ir\_1A}$, $i_{\rm ir\_1B}$, and $i_{\rm ir\_1C}$, which means that negative sequence 250 Hz currents are indeed universal.

C. Validations Regarding SP System

1) Simulation Test Based on Normal Conditions: To validate the coordination between SP DG units and TP DG units, a TP inverter is included in this test, and the test circuit is shown in Fig. 28.

According to Table I, 100 Hz and 250 Hz currents are tested, respectively. The simulation results are shown in Fig. 29, where

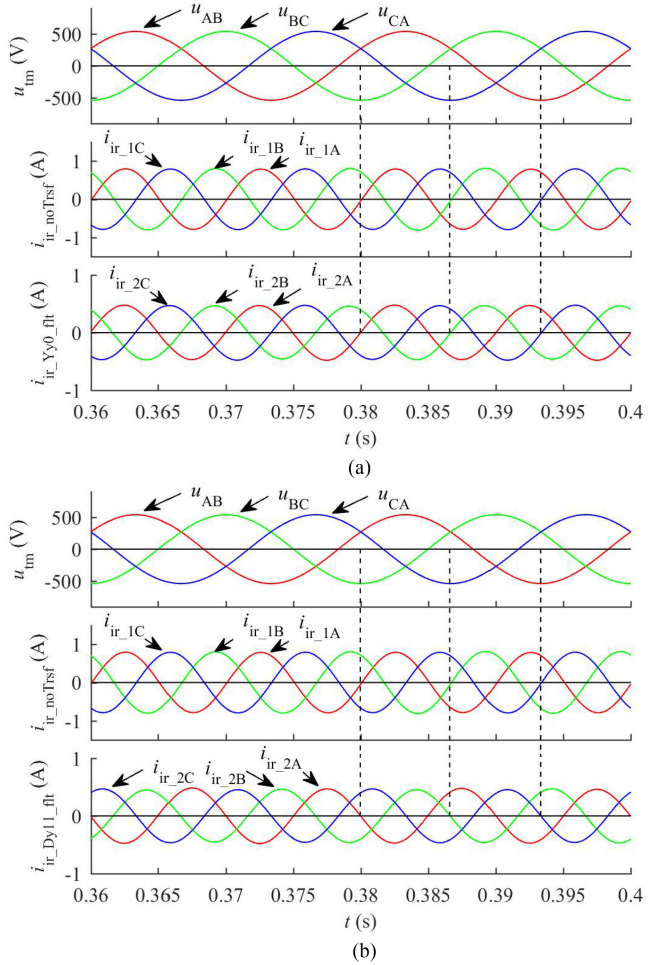

Fig. 26. Negative sequence 100 Hz currents waveforms based on a PSQF. (a) Transformer with Y,y0 connection. (b) Transformer with D,y11 connection.

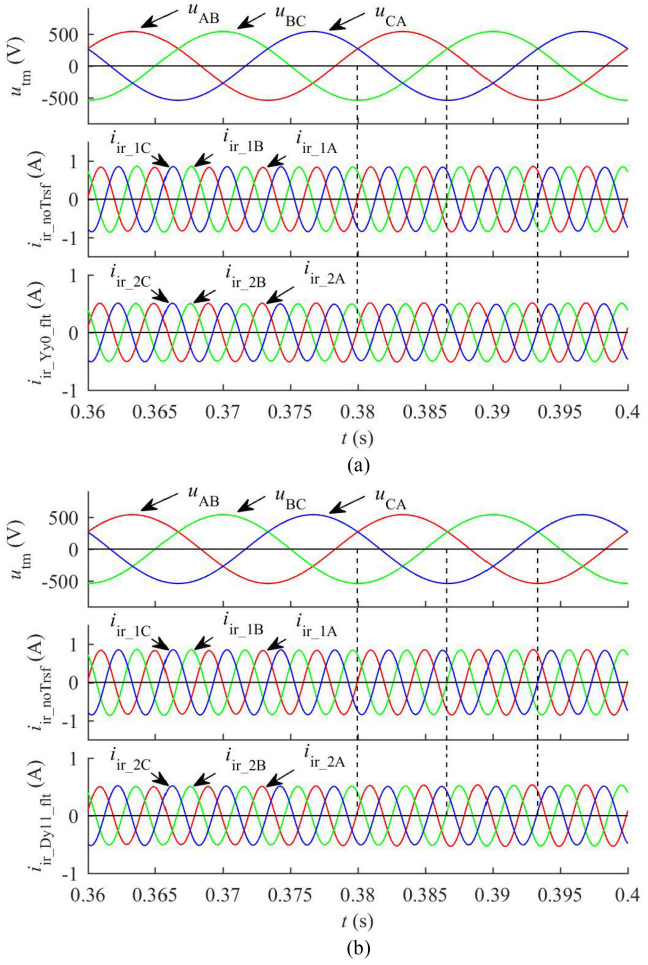

Fig. 27. Negative sequence 250 Hz current waveforms based on a PSQF. (a) Transformer with Y,y0 connection. (b) Transformer with D,y11 connection.

i_{ir_2A} and i_{ir_1s} represent the TP and SP irregular currents, respectively. It can be seen that i_{ir_1s} and i_{ir_2A} are in phase at the frequencies of both 100 Hz and 250 Hz, respectively, which demonstrates that the expected effect is reached.

2) Simulation Test Based on a PSBF: In this case, the test is based on the circuit in Fig. 30, where there is a PSBF at the primary side of the transformer.

As above, still 100 and 250 Hz currents are tested. The simulation results are shown in Fig. 31. In Fig. 31(b), when 250 Hz currents are injected, the injection effect is as well as that in Fig. 29(b), whereas, in Fig. 31(a), when 100 Hz currents are injected, i_{ir_1s} and i_{ir_2A} are almost out of phase.

In conclusion, 250 Hz currents can be used as injected currents while 100 Hz currents cannot in case of PSBFs. In other words, considering various scenarios, 250 Hz currents are universal for SP systems.

D. Validations Regarding the Conclusions Based on Actual Transformers

The simulation circuit is shown in Fig. 32. Negative sequence 100 Hz currents are still adopted and are extracted by band pass

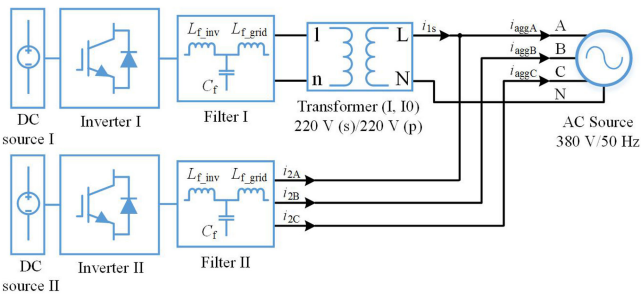

Fig. 28. Simulation circuit regarding SP system under normal conditions.

filters; both inverters I and II are based on unity power factor control and output 10 kW and 5 kW power, respectively, and the leakage impedance of the ideal transformer is set to zero, whereas for the actual transformer (rated power of 15 kVA), it is set as follows:

$$r_1 = 0.002 \text{ p.u.}, x_1 = 0.02 \text{ p.u.}, r_2 = 0.002 \text{ p.u.}, x_2 = 0.02 \text{ p.u.}$$

The simulation results are shown in Fig. 33. The primary and secondary irregular currents in the actual transformer

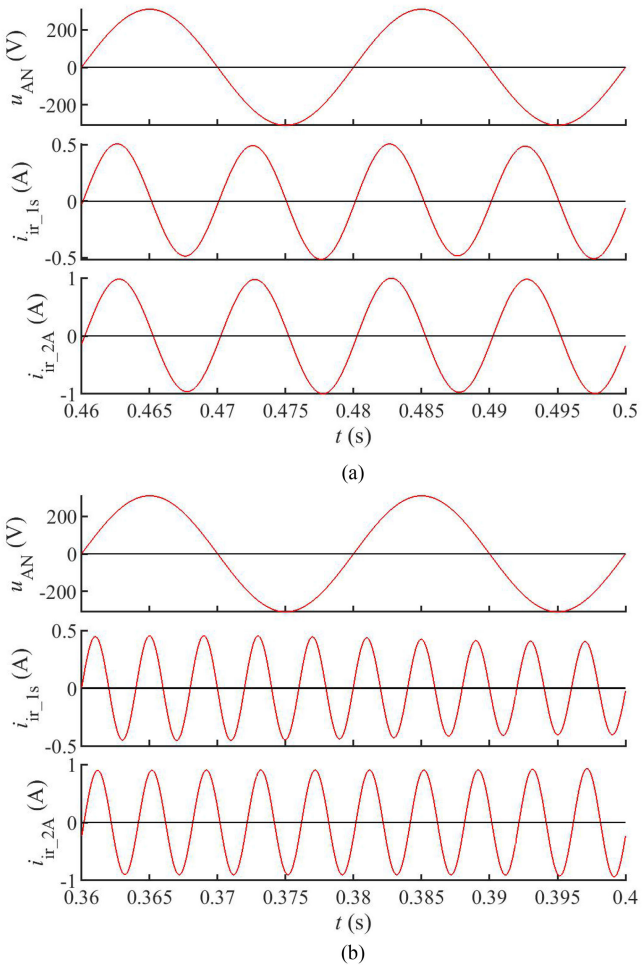

Fig. 29. SP and TP irregular current waveforms based on normal conditions. (a) 100 Hz currents (being of negative sequence for inverter II). (b) 250 Hz currents (being of negative sequence for inverter II).

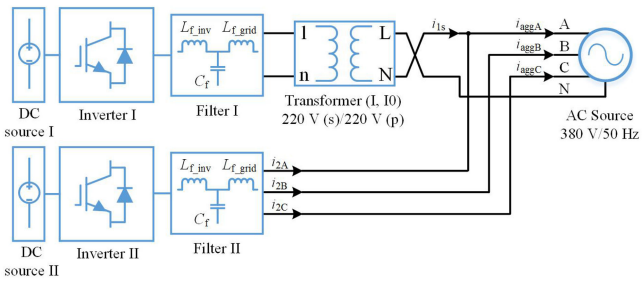

Fig. 30. Simulation circuit regarding SP system with a PSBF.

($i_{2h\_1A/B/C}$ and $i_{2h\_1a/b/c}$) lead those in the ideal transformer ($i_{2h\_2A/B/C}$ and $i_{2h\_2a/b/c}$), respectively, which is consistent with the conclusion in Section V.

In conclusion, all the experimental and simulation results are coincident with the conclusions in Sections III–V, which in particular verifies the accuracy of Table I. Accordingly, the solution to compatibility issues with irregular current injection methods proposed in this article is practicable and effective.

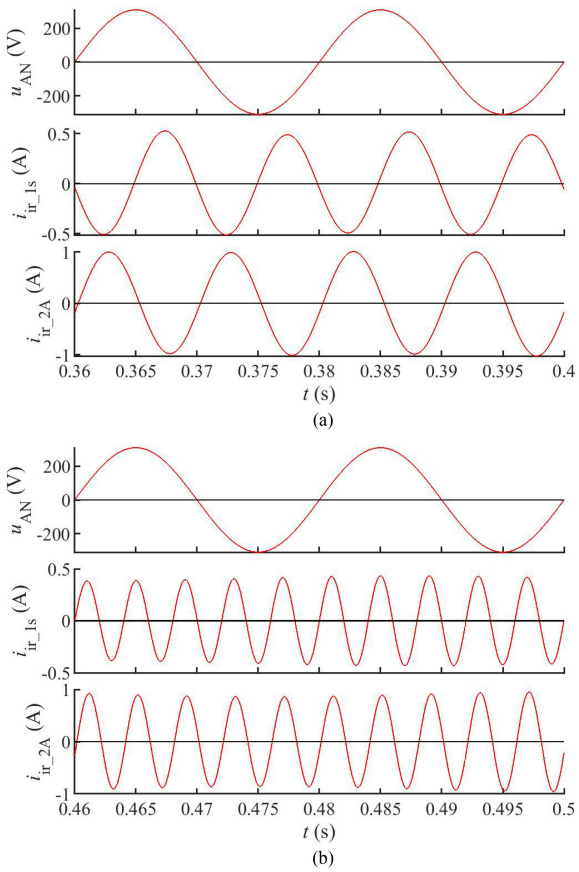

Fig. 31. SP and TP irregular currents waveforms based on a PSBF. (a) 100 Hz currents (being of negative sequence for inverter II). (b) 250 Hz currents (being of negative sequence for inverter II).

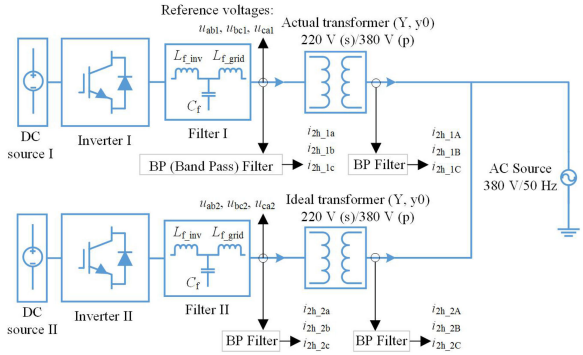

Fig. 32. Simulation circuit regarding an actual transformer.

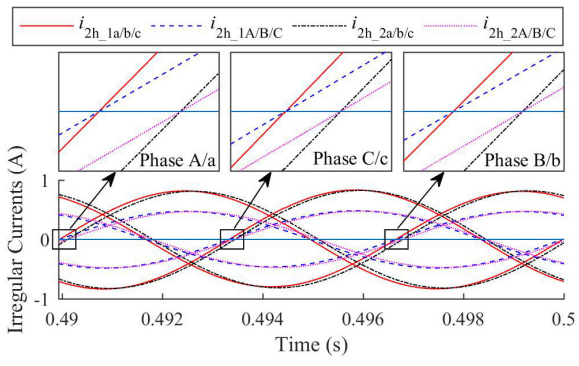

Fig. 33. Leading phase variations in the actual transformer.

VII. Conclusion

This article studies compatibility issues with irregular current injection islanding detection methods in multi-DG units equipped with grid-connected transformers. The issues require that the phase difference between any two irregular currents injected into the same line should be in $[-\pi/2, \pi/2]$ interval. According to this requirement, an injection pattern that uses terminal voltages of DG units to conduct irregular current injection is adopted. On the basis of this injection pattern, this article systematically analyzes how to meet the compatibility requirement when DG units are equipped with grid-connected transformers. As a result, the setting formulas of $T_{\rm lag}$ (i.e., $T_{\rm a\_tr}$ for TP DG units and $T_{\rm l\_tr}$ for SP DG units) and usable frequencies are derived, which are different from those based on direct couple conditions. Furthermore, it is found that to obtain fault tolerance and practicability, for irregular currents, only specific frequencies can be used and the usable frequencies are different under different faults, which are also different from those based on direct couple conditions.

All the conclusions based on conditions with grid-connected transformers achieved in this article and those based on direct couple conditions presented in the literature are summarized. Accordingly, a complete solution to compatibility issues with irregular current injection islanding detection methods is formed finally.

Irregular current injection is a critical link in irregular current injection islanding detection methods whose overall effect will greatly affect the subsequent links and even the islanding detection performance. This article not only proposes a complete solution to compatibility issues for the first time, but also shows the seriousness of the issues and the difficulty to solve the issues, whereby we hope that researchers, manufacturers, and grid code makers will pay attention to the issues and cooperate to solve them in practice.

References

[1] D. Voglitsis, N. Papanikolaou, and A. C. Kyritsis, "Incorporation of harmonic injection in an interleaved flyback inverter for the implementation of an active anti-islanding technique," *IEEE Trans. Power Electron.,* vol. 32, no. 11, pp. 8526–8543, Nov. 2017.

[2] A. Emadi, H. Afrakhte, and J. Sadeh, "Fast active islanding detection method based on second harmonic drifting for inverter-based distributed generation," *IET Gener., Transmiss. Distrib.,* vol. 10, no. 14, pp. 3470–3480, 2016.

[3] W. Cai, B. Liu, S. Duan, and C. Zou, "An islanding detection method based on dual-frequency harmonic current injection under grid impedance unbalanced condition," *IEEE Trans. Ind. Informat.,* vol. 9, no. 2, pp. 1178–1187, May 2013.

[4] A. Vijayakumari, A. T. Devarajan, N. Devarajan, and K. Vijith, "Dynamic grid impedance calculation in d-q frame for micro-grids," in *Proc. Power Energy Syst. Conf., Sustain. Energy*, Mar. 2014, pp. 13–15.

[5] Z. Wu, F. Yang, Z. Luo, and Q. L. Hang, "A novel active islanding fault detection based on even harmonics injection and set-membership filtering," in *Proc. 11th World Congr. Intell. Control Autom.*, 2015, pp. 3683–3689.

[6] M. Tedde and K. Smedley, "Anti-islanding for three-phase one-cycle control grid tied inverter," *IEEE Trans. Power Electron.,* vol. 29, no. 7, pp. 3330–3345, Jul. 2014.

[7] H. J. Kim, D. H. Kim, and B. M. Han, "Islanding detection method with negative-sequence current injection under unbalanced grid voltage," in *Proc. Future Energy Electron. Conf.*, 2015, pp. 1–6.

[8] Z. Dai, Z. Chong, X. Liu, and C. Li, "Active islanding detection method based on grid-connected photovoltaic inverter and negative sequence current injection," in *Proc. Int. Conf. Power System Technol.*, 2014, pp. 1685–1690.

[9] C.-C. Hou and Y.-C. Chen, "Active anti-islanding detection based on pulse current injection for distributed generation systems," *IET Power Electron.,* vol. 6, no. 8, pp. 1658–1667, 2013.

[10] D. D. Reigosa, F. Briz, C. B. Charro, and J. M. Guerrero, "Islanding detection in three-phase and single-phase systems using pulsating high-frequency signal injection," *IEEE Trans. Power Electron.,* vol. 30, no. 12, pp. 6672–6683, Dec. 2015.

[11] M. Khodaparastan, H. Vahedi, F. Khazaeli, and H. Oraee, "A novel hybrid islanding detection method for inverter-based DGs using SFS and ROCOF," *IEEE Trans. Power Del.,* vol. 32, no. 5, pp. 2162–2170, Oct. 2017.

[12] M. Liu, W. Zhao, S. Huang, Q. Wang, and K. Shi, "Problems in the classic frequency shift islanding detection methods applied to energy storage converters and a coping strategy," *IEEE Trans. Energy Convers.,* vol. 33, no. 2, pp. 496–505, Jun. 2018.

[13] J. Muñoz-Cruzado-Alba, J. Villegas-Núñez, J. A. Vite-Frías, J. M. Carrasco-Solís, and E. Galván-Díez, "New low-distortion Q–f droop plus correlation anti-islanding detection method for power converters in distributed generation systems," *IEEE Trans. Ind. Electron.*, vol. 62, no. 8, pp. 5072–5081, Aug. 2015.

[14] B. H. Kim and S. K. Sul, "Comparison of non-detection zone of frequency drift anti-islanding with closed-loop power controlled distributed generators," in *Proc. IEEE Int. Future Energy Electron. Conf.*, 2015, pp. 1–5.

[15] M. Liu, W. Zhao, Q. Wang, S. Huang, and K. Shi, "A solution to the parameter selection and current static error issues with frequency shift islanding detection methods," *IEEE Trans. Ind. Electron.*, vol. 68, no. 2, pp. 1401–1411, Feb. 2021.

[16] A. A. Abdelsalam, A. A. Salem, E. S. Oda, and A. A. Eldesouky, "Islanding detection of microgrid incorporating inverter based DGs using long short-term memory network," *IEEE Access*, vol. 8, pp. 106471–106486, 2020.

[17] B. K. Chaitanya, A. Yadav, and M. Pazoki, "Reliable islanding detection scheme for distributed generation based on pattern-recognition," *IEEE Trans. Ind. Informat.*, vol. 17, no. 8, pp. 5230–5238, Aug. 2021.

[18] M. Babakmehr, F. Harirchi, P. Dehghanian, and J. Enslin, "Artificial intelligence-based cyber-physical events classification for islanding detection in power inverters," *IEEE J. Emerg. Sel. Topics Power Electron.*, vol. 9, no. 5, pp. 5283–5293, Oct. 2021.

[19] P. P. Das and S. Chattopadhyay, "A voltage-independent islanding detection method and low-voltage ride through of a two-stage PV inverter," *IEEE Trans. Ind. Appl.*, vol. 54, no. 3, pp. 2773–2783, May/Jun. 2018.

[20] M. R. Alam, M. T. A. Begum, and B. Mather, "Islanding detection of distributed generation using electrical variables in space vector domain," *IEEE Trans. Power Del.*, vol. 35, no. 2, pp. 861–870, Apr. 2020.

[21] D. D. Reigosa, F. Briz, C. Blanco Charro, and J. M. Guerrero, "Passive islanding detection using inverter nonlinear effects," *IEEE Trans. Power Electron.*, vol. 32, no. 11, pp. 8434–8445, Nov. 2017.

[22] K. Colombage, J. Wang, C. Gould, and C. Liu, "PWM harmonic signature-based islanding detection for a single-phase inverter with PWM frequency hopping," *IEEE Trans. Ind. Appl.*, vol. 53, no. 1, pp. 411–419, Jan./Feb. 2017.

[23] V. R. Reddy and E. S. S., "A feedback-based passive islanding detection technique for one-cycle-controlled single-phase inverter used in photovoltaic systems," *IEEE Trans. Ind. Electron.*, vol. 67, no. 8, pp. 6541–6549, Aug. 2020.

[24] B. K. Choudhury and P. Jena, "Superimposed impedance based passive islanding detection scheme for DC microgrids," *IEEE J. Emerg. Sel. Topics Power Electron.*, to be published, doi: 10.1109/JESTPE.2021.3076459.

[25] Q. Huang, H. Chen, X. Xiang, C. Li, W. G. Li, and X. He, "Islanding detection with positive feedback of selected frequency for DC microgrid systems," *IEEE Trans. Power Electron.*, vol. 36, no. 10, pp. 11800–11817, Oct. 2021.

[26] M. Liu, W. Zhao, Q. Wang, S. Huang, and K. Shi, "Compatibility issues with irregular current injection islanding detection methods and a solution," *Energies,* vol. 12, no. 8, 2019, Art. no. 1467.

[27] W. Bower and M. Ropp, "Evaluation of islanding detection methods for utility-interactive inverters in photovoltaic systems," Off. Sci. Tech. Inf. Tech. Rep., Task V Report IEA PVPS T5-09: 2002, 2002.

[28] D. Voglitsis, F. Valsamas, N. Rigogiannis, and N. P. Papanikolaou, "On harmonic injection anti-islanding techniques under the operation of multiple DER-Inverters," *IEEE Trans. Energy Convers.*, vol. 34, no. 1, pp. 455–467, Mar. 2019.

[29] F. Valsamas, D. Voglitsis, N. Rigogiannis, N. Papanikolaou, and A. Kyritsis, "Comparative study of active anti-islanding schemes compatible with MICs in the prospect of high penetration levels and weak grid conditions," *IET Gener., Transmiss. Distrib.*, vol. 12, no. 20, pp. 4589–4596, 2018, doi: 10.1049/iet-gtd.2018.5636.

[30] *Electromagnetic Compatibility (EMC) - Part 3-3: limits - Limitation of Voltage Changes, Voltage Fluctuations and Flicker in Public Low-Voltage Supply Systems, for Equipment with Rated Current $<=$ 16 A Per Phase and Not Subject to Conditional Connection*, *IEC 61000-3-3:2013+A1*, 2021.

[31] C. Xue, L. Ding, and Y. R. Li, "Model predictive control with reduced common-mode current for transformerless current-source PMSM drives," *IEEE Trans. Power Electron.*, vol. 36, no. 7, pp. 8114–8127, Jul. 2021.

[32] C. Xue, L. Ding, Y. Li, and N. R. Zargari, "Improved model predictive control for high-power current-source rectifiers under normal and distorted grid conditions," *IEEE Trans. Power Electron.*, vol. 35, no. 5, pp. 4588–4601, May 2020.

[33] J. Azurza Anderson, G. Zulauf, P. Papamanolis, S. Hobi, S. Mirić, and J. W. Kolar, "Three levels are not enough: Scaling laws for multilevel converters in AC/DC applications," *IEEE Trans. Power Electron.*, vol. 36, no. 4, pp. 3967–3986, Apr. 2021.

[34] L. Zheng, R. P. Kandula, K. Kandasamy, and D. Divan, "Stacked low-inertia converter or solid-state transformer: Modeling and model predictive priority-shifting control for voltage balance," *IEEE Trans. Power Electron.*, vol. 36, no. 8, pp. 8934–8952, Aug. 2021.

[35] J. Hu and Y. He, "Modeling and control of grid-connected voltage-sourced converters under generalized unbalanced operation conditions," *IEEE Trans. Energy Convers.*, vol. 23, no. 3, pp. 903–913, Sep. 2008.

Menghua Liu received the B.Eng. degree in automatic control engineering from the Wuhan University of Science and Technology, Wuhan, China, in 2005, and the Ph.D. degree in electrical engineering from Tsinghua University, Beijing, China, in 2019.

He is currently an Assistant Research Fellow with the Guangzhou Institute of Energy Conversion, Chinese Academy of Sciences, Guangzhou, China. His research interests include the inverters/converters technology and applications in renewable energy generation.

Wei Zhao received the B.Eng. degree in electrical engineering from Tsinghua University, Beijing, China, in 1982, and the Ph.D. degree in electrical engineering from Moscow Power Engineering Institute, Moscow, Russia, in 1991.

He is currently a Professor with the Department of Electrical Engineering, Tsinghua University. His research interests include modern electromagnetic measurement and instrument techniques.

Qing Wang (Senior Member, IEEE) received the B.Eng. degree in electronic instrument and measurement technique from Beihang University, Beijing, China, in 1995, the M.Sc. degree in advanced manufacturing and materials from the University of Hull, Hull, U.K., in 1998, and the Ph.D. degree in manufacturing management from De Montfort University, Leicester, U.K., in 2001.

She is currently an Associate Professor with the Department of Engineering, Durham University, Durham, U.K. Her research interests include electronic instruments and measurement, computer simulation, and advanced manufacturing technology.

Zhiming Wang received the B.Eng. degree from Chongqing University, Chongqing, China, in 1996.

He is currently the Director of China Nuclear Power Design Co., Ltd., Shenzhen, China. His research interests include the design and system integration technology and management in renewable energy generation.

Caijun Jiang received the M.Eng. degree from Xi'an Jiaotong University, Xi'an, China, in 2004.

He is currently a Senior Engineer with China Nuclear Power Design Co., Ltd., Shenzhen, China. His research interests include the design technology and management in renewable energy generation.

Jie Shu received the B.S. degree in electric machines from the Shenyang University of Technology, Shenyang, China, in 1995, the M.S. degree in computer application from the South China University of Technology, Guangzhou, China, in 2004, and the Ph.D. degree in operations research and control theory from Sun Yat-sen University, Guangzhou, China, in 2009.

He is currently a Research Fellow, Chief of the Renewable Energy Generation and Microgrid Technology Laboratory with the Guangzhou Institute of Energy Conversion, Chinese Academy of Sciences, Guangzhou, China. His research interests include power electronics control and microgrid technology for renewable energy generation and building integrated photovoltaic.

Hao Wang received the B.S. and M.S. degrees in power electronics from the South China University of Technology, Guangzhou, China, in 1999 and 2002, respectively, and the Ph.D. degree in electric power engineering from Xi'an Jiaotong University, Xi'an, China, in 2011.

Since 2014, he has been a Research Assistant with the Guangzhou Institute of Energy Conversion, Chinese Academy of Sciences, Guangzhou, China. His research interests include distributed renewable energy generation and microgrid technology, power electronics in distributed power system, etc.

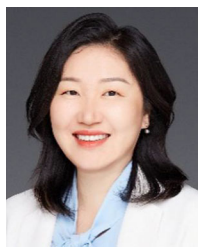

Yu Bai received the B.S. degree in environmental engineering from the South China University of Technology, Guangzhou, China, in 2003, and the M.S. degree in environmental engineering and sustainable architecture in 2005 and the Ph.D. in civil engineering and habitat science in 2009 from the University of Savoie Mont-Blanc, Chambéry, France.

She worked in the fields of hybrid solar thermal and photovoltaic systems, low-carbon building related technologies and optimization, energy strategy and low-carbon development. She was certified as "BEAM (Building Environment Assessment Method) Professional" by Hong Kong Green Building Council. She is currently the Deputy Director of Science and Technology Division, Guangzhou Institute of Energy Conversion, Chinese Academy of Sciences, Guangzhou, China, and has experience in promoting international cooperation.